國立臺灣大學醫學院生物化學暨分子生物研究所

博士論文

Graduate Institute of Biochemistry and Molecular Biology

College of Medicine

National Taiwan University

Doctoral Dissertation

抗癌藥物引發之人類第二型拓樸異構酶 α 亞型切割複

合體之結構分析：發展具亞型專一性之第二型拓樸異

構酶標靶抗癌藥物

Structural Studies of Human Topoisomerase IIα in Complexes

with DNA and Anticancer Drugs : Development of Selective

Topoisomerase II-Targeting Anticancer Drugs

王英任

Ying-Ren Wang

指導教授：詹迺立 博士

Advisor : Nei-Li Chan, Ph.D.

中華民國 106 年 9 月

Sep 2017

謝誌

這篇論文可以順利完成，完全要感謝我的指導老師詹迺立教授，在我博士班的這幾年用盡心力的指導，總是以鼓勵代替責罵把所有困難的事情攬在自己身上，無論如何都先以學生的利益為出發點，願意幫學生修改論文不眠不休的工作到凌晨，能成為詹迺立老師的學生是幸福的一件事，也謝謝老師提供了自己的肩膀，讓我可以站在巨人的肩上看的更遠更廣，也讓我見識到學無止境的認真努力態度。

博士班的這幾個年頭，謝謝我遇到過的所有學長姊：玉珍學姊、德昇學長、志強學長，學弟妹：甫甫、凱爾、阿毛、韋辰、香菇、阿咪老師、小胖舅、Kevin、一姊、蝦仁、君毅、可婷...等族繁不及備載。感謝大家參與在詹老師家的貢獻，忍受我的惡言相向，但是我們真的是數一數二的歡樂實驗室。

感謝我最親愛的家人，爸媽、大姊、二姊完全讓我沒有壓力的完成漫長的博士班生涯，你們不成材的弟弟終於可以畢業了，謝謝你們一直以來的支持，辛苦了。最後我要感謝我的老婆權娟，沒有妳耐心、細心的提供我這麼多的幫忙，我的論文可能還不知道在哪裡。謝謝妳全然的相信我，給我無比的鼓勵，讓我能夠撐完博士班學程。也謝謝妳的話：夫妻就是要好好的相互扶持，我會一輩子謹記在心的。

將此篇論文獻給所有幫助過我的人，有太多人要謝，那就謝天吧！

王 英 任　謹致於

台大醫學院生化所 Sep 2017

I

摘要

人類第二型拓樸異構酶 α 亞型（Top2α）和 β 亞型（Top2β）為目前常用於化學療法治療癌症的細胞標的蛋白。藉由影響酵素本身的催化反應，此類化療藥物增加第二型拓樸異構酶調控的 DNA 斷裂，並且造成 DNA 損傷以進而使細胞死亡，這些化療藥物有效的使第二型拓樸異構酶和 DNA 形成穩定的切割複合體。為了促進開發專一性藥物，我們成功解析了人類 Top2α 亞型酵素與 DNA 及抗癌藥物所形成的切割複合體晶體結構，在酵素與 DNA 的切割複合體中，清楚的看見藥物嵌入由酵素造成的 DNA 斷裂處。基於清楚的 Top2α 亞型結構資訊及實驗室先前對於 Top2β 亞型結構的研究探討，處於活性中心的胺基酸，甲硫氨酸（Methionine 762）在 Top2α 亞型及麩醯胺酸（Glutamine 788）在 Top2β 亞型具有氨基酸的差異性，可以做為設計藥物的參考。其中在 Top2α 亞型活性中心的甲硫氨酸可以用來設計與鉑（Platinum）衍生物產生鍵結，增加藥物嵌入 DNA 斷裂處的穩定度，進而生成更為穩定的酵素切割複合體。為了得到專一性藥物，我們設計並且獲得有機鉑化合物 （organoplatinum compound），藉由 cis-dichlorodiammineplatinum(II) 取代 etoposide 的糖官能基並且命名為 etoplatin-N2α、etoplatin-N2β。在 DNA 解超螺旋活性測試中，比起使用 etoposide 作為抑制物，對於 Top2α 亞型及 Top2β 亞型的解超螺旋活性 etoplatin-N2β 具有更好的抑制效果。在 Top2 調控的 DNA 斷裂實驗中，使用

etoposide 為抑制物，仍然有機會使 DNA 重新連接，而使用 etoplatin-N2β 為抑制物時，斷裂的 DNA 無法被有效的重新連接形成不可逆反應。藉由 Top2s 亞型酵素與 DNA 及 etoplatin-N2β 所形成的切割複合體晶體結構分析，etoplatin-N2β 的 Pt^{2+} 會與甲硫氨酸的 S^{δ} 產生穩定的配位鍵（coordinate bond）。然而當完整的藥物結合區域結構被破壞時，這個高度穩定 Pt^{2+}-S^{δ} 的配位鍵也會隨即斷裂，此一現象證明 Pt^{2+} 與酵素形成的配位鍵可以用來當成結構依賴型的藥物設計，使酵素抑制藥物具有可回復性。我們的實驗結果說明利用甲硫氨酸來針對 Top2α 亞型當成設計專一性藥物是可行的，並且可以減少藥物偏離目標結合至 Top2β 亞型造成的副作用。

Abstract

Human type II topoisomerase (Top2) isoforms, hTop2α and hTop2β, are the cellular

targets of some most successful drugs used in anticancer chemotherapy. By interfering

with the enzyme's catalytic cycle, these drugs promote Top2-mediated DNA cleavage to

trigger DNA damage-induced cell death pathways. The potency of these drugs relies on

effective stabilization of the enzyme-mediated DNA breaks. To facilitate drug

development, our lab had performed structural studies on hTopβ and revealed the actions

of Top2-targeting anticancer drugs. In this work, we have further determined the

structures of hTop2α cleavage core (hTop2α^{core}) in complexes with double strand DNA

and anticancer drugs. Structural analysis revealed the presence of a methionine residues,

Met762 and Met766, in the drug-binding pocket of hTop2α, allowing us to test whether

a tighter Top2-drug association may be accomplished by introducing a methionine-

directed, thioether-reactive Pt^{2+} into a drug to further stabilize the DNA break. To this

end, we designed and obtained an organoplatinum compound, called etoplatin-N2β, by

replacing the methionine-juxtaposing glycosidic group of etoposide with a cis-

dichlorodiammineplatinum(II) moiety. Comparing to etoposide, etoplatin-N2β more

potently inhibits the supercoil relaxation activity of hTop2α and hTop2β. While the

Top2-mediated DNA breaks arrested by etoposide can be rejoined, the breaks produced

in the presence of etoplatin-N2β are practically irreversible. Crystallographic analyses of

hTop2α and hTop2β cleavage complex stabilized by etoplatin-N2β demonstrate the

formation of a coordinate bond between Pt^{2+} and the S$^{\delta}$ atom of Met766 in the α-isoform

and the equivalent Met782 in β-isoform. Notably, this highly stable coordinate tether can

be loosened by disrupting the structural integrity of drug binding pocket with protein

denaturant, suggesting that the Pt^{2+} coordination chemistry may allow the development

of a potent enzyme inhibitor with protein conformation-dependent reversibility. Our

results also implicate selective targeting of an hTop2α-specific methionine (Met762) may

be achieved to suppress hTop2β-related side effects.

Keywords: human type II topoisomerases; topoisomerase-induced DNA break;

platinum(II)-thioether coordination; organoplatinum compound; protein conformation-

dependent reversibility.

Abbreviations

AML	Acute myeloid leukemia
C-gate	C-terminal gate
CTD	C-terminal domain
EVP	Etoposide
Gyrase	Bacterial DNA gyrase
G-DNA	Gate segment
hTop2α	Human topoisomerase IIα
hTop2α^{core}	DNA-binding and cleavage core of hTop2α
hTop2β	Human topoisomerase IIβ
hTop2β^{core}	DNA-binding and cleavage core of hTop2β
MLL	Mixed lineage leukemia gene
MIX	Mitoxantrone
PML	Promyelocytic leukemia gene
T-DNA	Transported segment
Top(s)	DNA topoisomerase(s)
Top1(s)	Type I DNA topoisomerase(s)
Top2(s)	Type II DNA topoisomerase(s)
Top2-cc	Top2 cleavage complex
Top IV	Bacterial DNA topoisomerase IV
TOPRIM domain	Topoisomerase-primase domain
Top V	DNA topoisomerase V
Top VI	DNA topoisomerase VI
VM26	Teniposide
WHD	Winged-helix domain
yTop2	Saccharomyces cerevisiae topoisomerase II
yTop2^{core}	DNA-binding and cleavage core of yTop2

Contents

List of Figures

x

List of Tables and Scheme

1. Introduction

1.1. DNA Topoisomerase and DNA topology problem

Cellular DNAs are extremely long polymers that play a critical role in carrying genetic information. DNA can be used as template for transcription to produce mRNA, and mRNA is then translated into protein to execute biological functions. In nature, DNA mostly exists in double-stranded form, the sequences of the two strands are complementary to each other and wound in a spiral. This DNA double helix structure can effectively store and transfer genetic information and protect the bases from being damaged by some harmful substances in the cell. When DNAs are involved in cellular processes such as replication, transcription and recombination, the base pairs embedded within the double helical structure need to be separated or disentangled. However, since cellular DNAs frequently exist as closed rings or become a part of large nuleoprotein complexes, free rotation of DNA is usually prohibited. As a result, separation of two intertwined DNA strands would induce compensatory winding and tangling known as DNA supercoils. This unwinding-induced formation of DNA supercoils is an example of DNA topological problem (1). The other commonly encountered DNA topological problems are DNA catenane and knots. For example, during DNA replication, movement of the replication fork would induce over-winding ahead of replication fork, that is, DNA is twisted into the tighter positive supercoils. If the accumulation of positive supercoils cannot be removed, the progression of replication fork would be inhibited, resulting in

2

premature termination of DNA replication. It addition, two replication forks would converge during the final stage of replication, and the newly synthesized DNA would become catenated (or interlinked) with template DNA. These DNA catenanes need to be properly segregated for being correctly distributed to daughter cells. Similarly, during transcription, the RNA polymerase accumulates positive supercoils ahead of the transcription bubble. Because the linking number associated with a closed DNA topological domain is fixed, therefore equal amount of negative supercoils would be generated behind RNA polymerase. The loosened DNA is at risk of being damaged or cleaved. Taken together, a number of DNA topological problems need to be resolved during cellular DNA transactions, otherwise a cell would not function properly and can even undergo cell death (2). In response to the various DNA topological problems faced by living organisms, a group of enzymes called DNA topoisomerases that are specialized in regulating DNA topology has evolved. These enzymes perform coordinated DNA cleavage and religation activity to regulate DNA topology and maintain the structural integrity of DNA (2, 3).

All DNA topoisomerase use the hydroxyl group of active site tyrosine to perform nucleophilic attack on the DNA main chain phosphodiester bond, this so-called transesterification reaction lead to DNA cleavage with concomitant formation of phosphotyrosyl bond. Thus, transient breaks can be introduced into DNA (2, 3), which

3

allows a second single or double strand to pass through the break. After this strand passage process is complete, DNA will be re-ligated to restore its structural integrity. This unique process catalyzed by topoisomerases can efficiently alter DNA topology.

The main activities of topoisomerases are to separate catananes resulted from replication and removing positive, negative supercoils to make DNA at free-energy stable state. However, a specialized topoisomerase called DNA gyrase in the prokaryote can relax positive supercoils and introduce negative supercoils into relaxed DNA. There is also a specialized topoisomerase termed reverse gyrase that is capable of introducing positive supercoils into DNA (4).

1.2. Classification and function of DNA Topoisomerase

According to their catalytic mechanisms, topoisomerases can be divided into two main categories, Type I topoisomerases cut one strand of a DNA double helix and Type II topoisomerases cut both DNA strands (5). These two types of topoisomerases can be further divided into Type IA、Type IB、Type IIA and Type IIB subfamilies by amino acid sequence homology, and it is generally recognizing that members of the same family of topoisomerase have similar structure and function. The Type IB forms covalent bond with DNA 3′ phosphate group. In contrast, the Type IA、Type IIA and Type IIB form DNA-enzyme covalent bond with 5′ phosphate group (3). A brief description of the different

4

types of topoisomerase function in cells is provided below.

Members of the Type IA topoisomerases include prokaryote Top I、Top III and eukaryote Top III, the main functions of these Type IA topoisomerase are relaxation of hyper-negatively supercoiled DNA and participate in DNA recombination and repair. Eukaryote Top I belongs to Type IB and is responsible for the removal of both positive and negative supercoils resulted from replication and transcription. Except for the specialized Type IA reverse gyrase that exists exclusively in the Archaea, the other Type IA enzymes do not require ATP for function (6).

Type IIA and Type IIB topoisomerases exhibit two-fold symmetric architecture (3), they can simultaneously cut both DNA strands to produce double strand break. Compared with the Type I topoisomerase, Type II topoisomerases utilize conformational changes induced by ATP binding and hydrolysis to drive another DNA duplex through the double-strand break, and then reseal the break to restore DNA integrity. The linking number will change ±2 in each complete catalytic cycle. The main functions of Type IIA include removal of positive or negative supercoils and unlinking of catenated DNA molecules cause by DNA replication to facilitate chromosome segregation. Type IIA is widely present in different organisms, both in the cells of bacteria, archaea and eukaryotic kingdom, and eukaryotic and bacterial cells contain at least one Type IIA enzyme (7). Base on protein sequence homology, type II enzymes can be further subdivided into

5

eukaryotic Top II、bacteria cells gyrase and Top IV. Although their mechanism of action

is similar, but each subfamily has its own unique features and plays distinct roles in cell

(8). Type IIB mainly exists in archaea, but it has also been found in plants and certain

bacteria and algae, with Top VI being the lone member (7). Type IIB can remove positive

and negative supercoils and decatenates interlinked DNA molecules like Type IIA (9),

and structurally it resembles Type IIA with similar functional domains. However, there

are many differences between these two Type II Tops. To date, the physiological function

of Top VI in eukaryotic cells is not clear, but sequence comparison revealed that it is

related to the meiosis recombination factor SPO11 (10).

1.3. The structure and molecular mechanism of Type IIA topoisomerase

Type IIA topoisomerases are multi-domain proteins with a two-fold symmetric

architecture. Starting from the N-terminus, the eukaryotic enzyme is composed of the

following domains: ATPase domain, transducer domain, Toprim (topoisomerase-primase)

domain, winged-helix domain (WHD), tower domain, coiled-coil region and C-terminal

domain (CTD). Except for the CTD, all Type IIA enzymes share high degree of sequence

homology and similar protein structure (11, 12). Between different species, the

aforementioned domain arrangement may differ. The eukaryotic Top2s function as

homodimers. In contrast, the prokaryotes DNA gyrase and Top IV compose of two

6

polypeptides and exist as A_2B_2 hetrotetramers (13).

The quaternary structure of Type IIA reveals the presence of three interfaces between the two subunits, corresponding to the three molecular gateways. The three gates are referred as the N-gate (entrance-gate), DNA-gate, and C-gate (exit-gate). The N-gate is composed of GHKL (Gyrase、Hsp90、Histidine kinase and Mut L) ATPase domain and transducer domain (14). The ATPase domain is responsible for ATP binding and hydrolysis, and the opening and closure of gate is controlled by ATP binding (15). The transducer domain is attached to the C-terminus of ATPase domain, and link the ATPase domain and to the DNA-gate. The transducer domain is thought to mediate allosteric interactions between the DNA-gate and ATPase domain (16). DNA-gate is responsible for DNA binding and cleavage. It is composed of a Mg^{2+} binding Toprim domain, WHD domain that harbors a DNA binding motif and catalytic tyrosine, and tower domain. The three domain collectively referred as DNA-binding and cleavage corer (DBCC). The Toprim domains are widely present in enzymes that catalyze hydrolysis of phosphodiester bond. This domain contains a DXD motif for binding divalent cation, typically a Mg^{2+}, as a catalytic cofactor. WHD shares structural similarity with the *E. coli* catabolite activation protein (CAP) DNA binding area, and is also referred to as the CAP-like domain. The Toprim domain and WHD interact with each other and with DNA, which positions the catalytic tyrosine for cleaving DNA. In addition, the tower domain extend

7

from WHD c-terminal also plays a role in DNA binding and may stabilize the bent conformation of DNA. The C-gate or exit-gate is located at the c-terminus of DBCC and is composed of two helices forming coiled-coil conformation, this area is important for maintaining the enzyme's unique tertiary structure and controls the release of DNA. Type IIA topoisomerase functions by coordinating the opening and closing of these gates to guide the cleavage and transportation of DNA. Through the results obtained from extensive structural analysis and biochemical experiments, it has been established that Top2 operates via the two-gate mechanism (17-20). According to this mechanism, the Type IIA topoisomerase first binds to and creates a gate on the G (gate)-segment DNA using its DBCC to allow the passage of a second DNA duplex, the T (transfer)-segment to be passed through the DNA-gate. Specifically, the catalytic cycle involves the following steps: 1. The G-segment passes through an opened N-gate and binding with DBCC. 2. After two ATP molecules bind to ATPase domain, the N-gate closes to capture T-segment and temporarily store it in cavity above the DNA-gate. 3. The G-segment is cleaved by the catalytic tyrosine, and hydrolysis of an ATP molecule triggers the protein conformation change to push the T-segment through the DNA break into the cavity under DNA-gate. 4. The G-segment is re-ligated to close the DNA-gate, and then the C-gate opens to release T-segment. 5. The second ATP molecule will be hydrolyzed to open the N-gate, which resets the protein to the origin state for next catalytic cycle. By this

8

mechanism, Type IIA topoisomerase would consume two ATP molecules during each round of DNA topological transformation.
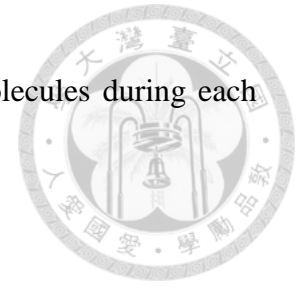
1.4. Human type IIA topoisomerase

There are two isoforms of type II topoisomerase (Top2α and Top2β) express in human cell (6, 12, 21-24). These topoisomerase isoforms are encoded by different genes (chromosome bands 17q21-22(α) and 3p24(β) in human) and share high overall sequence identity (~70%). Although the catalytic activities of Top2α and Top2β are similar, these isoforms are expressed in different phases of the cell cycle (6, 12, 21-24). Top2α is highly expressed in proliferating cells and essential for cell growth. In the rapidly proliferating cells contains as much as 500,000 copies of this Top2 isoform. During Mitosis, Topoisomerase IIα bound with replication forks and remains tightly associated with chromosomes (6, 12, 21-26), and is required for chromosome segregation.

Earlier studies revealed that Top2β is required for neural development in mammals, but it cannot compensate for Top2α loss in human cells (6, 12, 21-24, 27, 28), In addition, Top2β expresses at high levels in most cell types, but its concentration is independent of proliferation status (6, 12, 21-25). Top2β plays a critical role in the transcription of hormonally and regulated development genes (6, 26, 29, 30).

9

1.5. Type IIA topoisomerase poison and side effect

Top2 resolves topological entanglements in DNA by first catalyzing the formation of a transient covalent enzyme-DNA adduct termed Top2 cleavage complex (Top2cc), which harbors a double-strand DNA break to allow the following passage of another DNA segment (6, 12, 22-24). A number of clinically active anticancer drugs arrest the transiently formed Top2cc to exploit its latent yet lethal cytotoxicity; subsequent collision between the trapped Top2cc and DNA-tracking activities generates bulky DNA lesion and in turn causes cancer cell death (31-33).

Topoisomerase II poisons are used for clinical anticancer therapy (22, 23, 31-35). To date, there are six of topoisomerase II poisons approved in the United States. The anticancer drug produced from synthetic compounds or natural extract compound, all of them treat to variety human malignancies (22, 23, 31-35). The clinical anticancer drug such as etoposide and doxorubicin are used for solid tumors、leukemia、lymphoma、sarcomas、breast cancers、lung cancers、neuroblastoma and germ-cell malignancies. In addition, mitoxantrone is used to treat breast cancer、acute myeloid leukemia (AML)、non-Hodgkin lymphoma and multiple sclerosis (36). Many studies reported that topoisomerase II associated anticancer drugs target on both isoforms (23, 31-33, 35, 37). Furthermore, there are no isoforms-specific drugs for clinical used at the present time. The stronger side-effect will cause by target on the wrong isoform, For example, when

10

patients treat with the doxorubicin or mitoxantrone have does-limiting toxicity for cardiotoxicity (38, 39). The present study demonstrated that deletion of topoisomerase IIβ from cardiomyocyte protected doxorubicin-induced DNA damage at mouse hearts. Thus, it is conceivable that anticancer drug target on topoisomerase IIβ results in cardiotoxicity (40, 41). Moreover, numerous reports have documented that some topoisomerase II-associated secondary malignancies caused by anticancer drugs non-specific target on topoisomerase IIβ (30, 40, 42). It is also note that topoisomerase II isoforms are the targets for anticancer drug, and it have been linked to generation secondary leukemia (42-45). For example, the *MLL*(mixed lineage leukemia) and *PML*(promyelocytic leukemia) gene are most closely related to topoisomerase II in cancers(22, 23, 42-45).

1.6. Topoisomerase II-Mediated DNA Breaks by Site-Specific Pt(II)-Methionine Coordination Chemistry

Imbalances in enzyme activity are etological factors for numerous diseases, including inflammation, metabolic disorders, cardiovascular irregularities, and cancers. Therefore, modulation of enzyme function by bioactive small molecules is a commonly employed therapeutic strategy, and many successful drugs are enzyme inhibitors or poisons (46). The majority of drugs bind their targets via non-covalent forces, rendering

the interactions reversible in nature. In contrast, irreversible inhibition has been achieved

mainly via covalent bond formation between an inhibitor and its target (47-49). Despite

the superior *in vitro* potency displayed by these so-called covalent inhibitors, their

broader clinical applications are usually limited by pronounced adverse effects due to off-

target reactivity and potential immunogenicity arising from the resulting protein-inhibitor

adducts (50-52). Knowing that the stability of coordination complexes is determined in

part by the number and geometric distribution of metal-coordinating ligands, we

envisioned that the coordination bond formed between a transition metal ion incorporated

in an organic scaffold and reactive side chain functional group(s) in a target protein may

exhibit conditional liability. Perturbing the conformational state of the target protein may

alter the spatial arrangement of ligands, leading to rupture of the coordination linkage.

From previous studies, it was found that structural analyses revealed drug

intercalation between the base pairs flanking the DNA cleavage site, which effectively

stabilizes Top2cc by blocking religation of the cleaved DNA ends (53, 54). The

specificity displayed by these drugs towards the Top2-induced DNA cleavage site can be

rationalized by their interactions with the surrounding protein residues. The presence of

methionine residue(s) in the drug binding pocket in the two human Top2 isoforms,

hTop2α and hTop2β, suggests that site-specific incorporation of a Pt^{2+} reactive center into

a drug may enable the formation of a Pt^{2+}-thioether bond with the methionine side chain

12

(55) and boost the drug's efficacy by strengthening its interaction with human Top2cc.

The Top2-targeting anticancer drug etoposide is an ideal candidate for testing this concept

due to the well comprehended structure-activity relationships regarding its three

constituting moieties (56-59).

Here, we performed structure-based development of an etoposide derivative

containing a dichloroplatinum(II) moiety to show the generally irreversible and thus

highly efficient enzyme-targeting based on the Pt^{2+} coordination chemistry may become

dissociable upon protein unfolding, which demonstrates a potential benefit of employing

metal coordination chemistry in drug development.

13

2. Methods and Materials
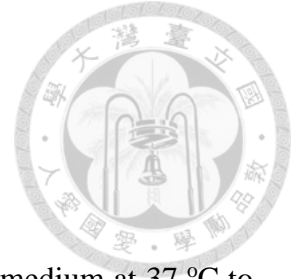
2.1. Protein Purification

Protein Expression and Preparing

For expression human Top2α ^{core}, after bacterial growth in LB medium at 37 ^{o}C to OD $_{600}$ = 0.5, isopropyl β-D-1-thiogalactopyranoside (IPTG) was added to a final concentration of 0.3 mM, and protein expression was induced at 16 ^{o}C for 16 hours. Bacteria were harvested centrifugation and stored at -80 ^{o}C. The cell pellet was resuspended in lysis buffer (50 mM sodium phosphate pH 7.4, 10% glycerol, 500 mM sodium chloride, 5 mM β-mercaptoethanol, 0.5 mM phenylmethanesulfonyl fluoride (PMSF), and 10 mM Imidazole), and the cells were disrupted by sonication. The crude cell extract was centrifuged at 18,000 rpm for 140 mins at 4 ^{o}C and applied to a Ni-NTA column.

For expression human Top2β ^{core}, after bacterial growth in LB medium at 37 ^{o}C to OD $_{600}$ = 1.0, TPTG was added to a final concentration of 0.3 mM, and protein expression was induced at 20 ^{o}C for 16 hours. Bacteria were harvested centrifugation and stored at -80 ^{o}C. The cell pellet was resuspended in lysis buffer (50 mM sodium phosphate pH 7.4, 10% glycerol, 500 mM sodium chloride, 5 mM β-mercaptoethanol, 0.5 mM PMSF, and 10 mM Imidazole), and the cells were disrupted by sonication. The crude cell extract was centrifuged at 18,000 rpm for 140 mins at 4 ^{o}C and applied to a Ni-NTA column.

For expression human Top2$\alpha$$^{FL-\triangle CTD}$, streaked human Top2$\alpha$$^{FL-\triangle CTD}$/BCY123 on

15

Ura⁻ plate and incubated for 2 days at 30 °C. Choose the single colony to incubate 100 ml

SD-U media shake at 30 °C for overnight. Used 10 ml of overnight cultures to inoculate

1L SD-U media incubated at 30 °C for overnight. After two times activated, harvested

cells by centrifugation and resuspended in 100 ml YPG media. Then assign 100 ml YPG

media into 10 L YPG media incubated 30 °C for 24 hrs. Harvested cells by centrifugation

and resuspended in lysis buffer (50 mM sodium phosphate pH 7.4, 10% glycerol, 500

mM sodium chloride, 5 mM β-mercaptoethanol, 0.5 mM PMSF, and 1 mM EDTA). The

cells were disrupted by bead-beater. The crude cell extract was centrifuged at 20,000 rpm

for 180 mins at 4 °C and applied to a Biorex 70 column.

For expression human Top2$\beta^{FL-\triangle CTD}$, streaked human Top2$\alpha^{FL-\triangle CTD}$/BCY123 on

Ura⁻ plate and incubated for 2 days at 30 °C. Choose the single colony to incubate 100 ml

SD-U media shake at 30 °C for overnight. Used 10 ml of overnight cultures to inoculate

1L SD-U media incubated at 30 °C for overnight. After two times activated, harvested

cells by centrifugation and resuspended in 100 ml YPG media. Then assign 100 ml YPG

media into 10 L YPG media incubated 30 °C for 24 hrs. Harvested cells by centrifugation

and resuspended in lysis buffer (50 mM sodium phosphate pH 7.4, 10% glycerol, 500

mM sodium chloride, 5 mM β-mercaptoethanol, 0.5 mM PMSF, and 1 mM EDTA). The

cells were disrupted by bead-beater. The crude cell extract was centrifuged at 20,000 rpm

for 180 mins at 4 °C and applied to a Biorex 70 column.

16

Liquid Chromatography

The human Top2 α^{core} protein sample was loaded into Ni-NTA column, the column was washed to baseline, and the protein was eluted with elution buffer (lysis buffer containing 250 mM Imidazole). The resulting protein sample was dialyzed against buffer A (30 mM Tris-HCl pH 7.5, 15 mM sodium chloride, 2 mM β-mercaptoethanol, and 1 mM EDTA) at 4 °C for 4 hours and loaded onto a HiPrep 16/10 Heparin FF column. The protein was eluted in a linear gradient over 10 column volumes with buffer (buffer A containing 1 M sodium chloride). The eluted fraction were pooled and purified on a size-exclusion column (Hi-Load Superdex 200) in gel filtration buffer (50 mM Tris-HCl pH 7.0, 200 mM KCl, 5 mM MnCl$_2$, 1 mM EDTA and 2 mM β-mercaptoethanol). The dimer-form protein (functional hTOP2A$^{\text{core}}$, with MW ~180 kDa) was collected and concentrated to 8 mg/ml for crystallization.

The human Top2 β^{core} protein sample was loaded into Ni-NTA column, the column was washed to baseline, and the protein was eluted with elution buffer (lysis buffer containing 250 mM Imidazole). The resulting protein sample was dialyzed against buffer A (30 mM Tris-HCl pH 7.5, 15 mM sodium chloride, 2 mM β-mercaptoethanol, and 1 mM EDTA) at 4 °C for 4 hours and loaded onto a HiPrep 16/10 Heparin FF column. The protein was eluted in a linear gradient over 10 column volumes with buffer (buffer A

17

containing 1 M sodium chloride). The eluted fraction were pooled and purified on a size-exclusion column (Hi-Load Superdex 200) in gel filtration buffer (buffer A containing 70 mM sodium chloride). The dimer-form protein (functional hTop2β^{core}, with MW ~180 kDa) was collected and concentrated to 6.5 mg/ml for crystallization.

The human Top2α$^{FL-\triangle CTD}$ protein sample was loaded into Biorex 70 column, the column was washed to baseline, and the protein was eluted with elution buffer (lysis buffer containing 1 M sodium chloride) in a linear gradient over 10 column volumes. The eluted fractions were pooled and purified on a size-exclusion column (Hi-Load Superdex 200) in a gel filtration buffer (50 mM Tris-HCl pH 7.5, 200 mM KCl, 2 mM β-mercaptoethanol, 5 mM MnCl$_2$ and 1 mM EDTA). The dimer-form protein (functional hTop2α^{core}, with MW ~276 kDa) was collected and concentrated to 1.2 μg/μl and 20 ng/μl for protein assay.

The human Top2β$^{FL-\triangle CTD}$ protein sample was loaded into Biorex 70 column, the column was washed to baseline, and the protein was eluted with elution buffer (lysis buffer containing 1 M sodium chloride) in a linear gradient over 10 column volumes. The eluted fractions were pooled and purified on a size-exclusion column (Hi-Load Superdex 200) in a gel filtration buffer (50 mM Tris-HCl pH 7.5, 200 mM KCl, 2 mM β-mercaptoethanol, 5 mM MnCl$_2$ and 1 mM EDTA). The dimer-form protein (functional hTop2α^{core}, with MW ~276 kDa) was collected and concentrated to 1.2 μg/μl and 20 ng/μl

for protein assay.
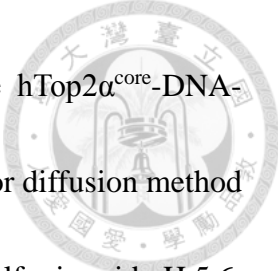
2.2. DNA Substrate for Crystallography

The design of the oligonucleotide sequence 5'-AGCCGAGCTGCAGCTCGGCT-3'

(Omics Bio) of the double-strand DNA substrate was based on the cleavage pattern of

human Top2 treated with anticancer drugs Etoposide (VP16, EVP), Teniposide (VM26)

and Mitoxantrone (MIX). The oligonucleotide were dissolved in buffer containing 30 mM

Tris-HCl pH 7.5, 70 mM sodium chloride, 2 mM β-mercaptoethanol, and 1 mM EDTA

and annealed at 55 ºC to generate double-stranded DNA for crystallization.

2.3. Crystallization

Crystallization of Human Top2α^{core}-DNA-Etoposide Ternary Complex

The human Top2α ^{core} protein sample was mixed with 1 mM etoposide (in DMSO)

and substrate (in a 1.2-fold molar ration to protein). Initial crystallization trials for the

hTop2α^{core}-DNA-Etoposide ternary complex were performed with commercially

available kits (Hampton Research) using the hanging drop vapor diffusion method.

Specifically, 1 µl of concentrated hTop2α^{core}-DNA-Etoposide solution in gel filtration

buffer was mixed an equal amount of reservoir solution and equilibrated against 200 µl

of reservoir solution at 4 ºC. Conditions that produced small crystal were refined by

19

systematic variation of the precipitant concentration and pH. The hTop2α^{core}-DNA-Etoposide ternary complex was crystallized by the hanging-drop vapor diffusion method using 100 mM magnesium acetate, 50 mM 2-(N-morpholino)ethanesulfonic acid pH 5.6, and 26% 2-methyl-2,4-pentanediol (MPD) as the precipitating agent. Single crystals suitable for data collection usually appear within two weeks. Crystal were harvested by transferring into mother liquor containing 30% MPD before looping and flash-freezing in liquid nitrogen for data collection. The hTop2α^{core}-DNA-Teniposide and hTop2α^{core}-DNA-Mitoxantrone ternary complex crystallization method as same as hTop2α^{core}-DNA-Etoposide ternary complex.

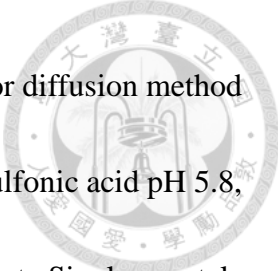### *Crystallization of Human Top2β^{core}-DNA-Etoposide Ternary Complex*

The human Top2β^{core} protein sample was mixed with 1 mM etoposide (in DMSO) and substrate (in a 1.2-fold molar ration to protein). Initial crystallization trials for the hTop2β^{core}-DNA-Etoposide ternary complex were performed with commercially available kits (Hampton Research) using the hanging drop vapor diffusion method. Specifically, 1 μl of concentrated hTop2β^{core}-DNA-Etoposide solution in gel filtration buffer was mixed an equal amount of reservoir solution and equilibrated against 200 μl of reservoir solution at 4 ºC. Conditions that produced small crystal were refined by systematic variation of the precipitant concentration and pH. The hTop2β^{core}-DNA-

20

Etoposide ternary complex was crystallized by the hanging-drop vapor diffusion method using 100 mM magnesium acetate, 50 mM 2-(N-morpholino)ethanesulfonic acid pH 5.8, and 22% 2-methyl-2,4-pentanediol (MPD) as the precipitating agent. Single crystals suitable for data collection usually appear within two weeks. Crystal were harvested by transferring into mother liquor containing 30% MPD before looping and flash-freezing in liquid nitrogen for data collection.

2.4. Post-Crystallization Drug Replacement

To obtain the hTop2α^{core} cleavage complex stabilized by Teniposide, Mitoxantrone was soaked out by transferring the hTop2α^{core}-DNA-Mitoxantron crystal into mother liquor containing 30% MPD for 16 hours. Teniposide then were soaked in by adding 1 mM drug (in DMSO) to the drop containing drug-free crystals for 16 hours. All crystals were harvested by transferring into mother liquor containing 30% MPD before looping and flash-freezing in liquid nitrogen for data collection.

To obtain the hTop2β^{core} cleavage complex stabilized by Etoplatin N2β and Etoplatin N2α, Etoposide was soaked out by transferring the hTop2β^{core}-DNA-Etoposide crystal into mother liquor containing 30% MPD for 16 hours. Etoplatin N2β and Etoplatin N2α then were soaked in by adding 1 mM drug (in DMSO) to the drop containing drug-free crystals for 16 hours. All crystals were harvested by transferring into mother liquor

21

containing 30% MPD before looping and flash-freezing in liquid nitrogen for data

collection.

2.5. Data Collection and Structure Determine

The hTop2α^{core}-DNA-Etoposide Ternary Complex

The diffraction data on the hTop2α^{core}-DNA-Etoposide complex were collected at

NSRRC, Taiwan (beamline BL13B1) and were processed using the HKL2000 program

suite (60). Structure was solved by molecular replacement with the PHENIX AutoMR

(using the drug free structure of hTop2β^{core}-DNA-Etoposide (PDBid : 3QX3) (53)) follow

by model building with PHENIX AutoBuild (61). The resulting electron density map

showed clearly the densities of the bound DNA and Etoposide, the structure of drug were

built into the density using Coot (62). Structure then underwent rounds of manual model

rebuilding and refinement with Coot and PHENIX. One cleavage complex molecule was

present in the asymmetric unit. Detailed refinement parameters are listed in **Table 1**. The

figure were generated in Pymol (63).

The hTop2α^{core}-DNA-Mitoxantrone Ternary Complex

The diffraction data on the hTop2α^{core}-DNA-Mitoxantrone complex were

collected at Spring-8, Japan (beamline BL12B2) and were processed using the HKL2000

22

program suite (60). Structure was solved by molecular replacement with the PHENIX AutoMR (61) (using the drug free structure of hTop2α^{core}-DNA-Etoposide). The resulting electron density map showed clearly the densities of the bound DNA and Mitoxantrone, the structure of drug were built into the density using Coot (62). Structure then underwent rounds of manual model rebuilding and refinement with Coot and PHENIX. One cleavage complex molecule was present in the asymmetric unit. Detailed refinement parameters are listed in **Table 2**. The figure were generated in Pymol (63).

The hTop2α^{core}-DNA-Teniposide Ternary Complex

The diffraction data on the hTop2α^{core}-DNA-Teniposide complex were collected at NSRRC, Taiwan (beamline BL13B1) and were processed using the HKL2000 program suite (60). Structure was solved by molecular replacement with the PHENIX AutoMR (61) (using the drug free structure of hTop2α^{core}-DNA-Etoposide). The resulting electron density map showed clearly the densities of the bound DNA and Mitoxantrone, the structure of drug were built into the density using Coot (62). Structure then underwent rounds of manual model rebuilding and refinement with Coot and PHENIX. One cleavage complex molecule was present in the asymmetric unit. Detailed refinement parameters are listed in **Table 2**. The figure were generated in Pymol (63).

The Drug-Bound hTop2α^{core} Cleavage Complex Derived by the Post-Crystallization Drug Replacement Procedure

The diffraction data on the hTop2α^{core}-DNA-Teniposide complex were collected at NSRRC, Taiwan (beamline BL13B1) and were processed using the HKL2000 program suite (60). Structure was solved by molecular replacement with the PHENIX AutoMR (61) (using the drug free structure of hTop2α^{core}-DNA-Mitoxantrone). The resulting mF_o-DF_c difference electron map of Teniposide-soaking in structure showed the presence of drug at the two DNA cleavage sites, the structure of drugs were built into the difference density map using Coot (62). The structure then underwent rounds of manual model rebuilding and refinement with Coot and PHENIX. Detailed refinement parameters are listed in **Table 2**. The figure were generated in Pymol (63).

The Drug-Bound hTop2β^{core} Cleavage Complexes Derived by the Post-Crystallization Drug Replacement Procedure

The diffraction data on the hTop2β^{core}-DNA-Etoplatin N2β and hTop2β^{core}-DNA-Etoplatin N2α complex were collected at NSRRC, Taiwan (beamline BL15A1) and were processed using the HKL2000 program suite (60). Structure was solved by molecular replacement with the PHENIX AutoMR (61) (using the drug free structure of hTop2β^{core}-DNA-Etoposide (PDBid : 3QX3) (54)). The resulting mF_o-DF_c difference electron map

24

of Etoplatin N2β- and Etoplatin N2α-soaking in structure showed the presence of drug at

the two DNA cleavage sites, the structure of drugs were built into the difference density

map using Coot (62). The structure then underwent rounds of manual model rebuilding

and refinement with Coot and PHENIX (61). Detailed refinement parameters are listed in

Table 1. The figure were generated in Pymol (63).

Structural modeling of etoplatin-stabilized hTop2α cleavage complexes

Structural models were constructed by first replacing the bound etoposide molecules

in the crystal structure of hTOP2α^{core}-DNA-etoposide with etoplatin-N2β and N2α,

respectively, under the assumption that the aglycone core and E-ring of the two

compounds (**Figure 12**) share the same binding mode. The linker that connects the

reactive dichlorodiammineplatinum(II) moiety to the aglycone C-ring was also assumed

to adopt the conformation observed in the crystal structures of hTop2β^{core}-DNA-etoplatin-

N2β and hTop2β^{core}-DNA-etoplatin-N2α complexes. Next, all energetically accessible

rotamers of the hTOP2α-specific M762 were surveyed to identify side-chain

conformations that allow its S^{δ} to overlay on and substitute for one of the Cl^{-} ions of the

dichlorodiammineplatinum(II) moiety as a ligand for Pt^{2+}. The Pt^{2+}-S^{δ} bond length was

then restrained at ~2.3 Å during subsequent energy minimization using the "In Situ

Ligand Optimization" and "Calculate Binding Energies" modules of Discovery Studio

25

4.1 to idealize the drug binding mode. For the additionally designed Pt^{2+} derivatives, structural modeling was conducted using the same procedure except that the conformations of the linker and the M762 side-chain were both adjusted to allow the formation of Pt^{2+}-S^{δ} bond.
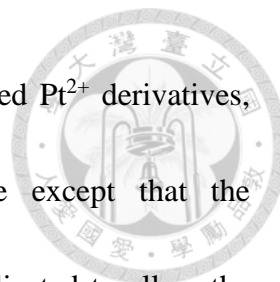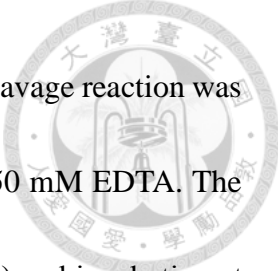
2.6. Protein assay

Topoisomerase DNA Relaxation Assay

The supercoil relaxation reaction (20 μl) was conducted at 37ºC for 30 minutes in a buffer containing 10 mM Tris-HCl pH 8.0, 100 mM KCl, 0.1 mM EDTA, 5 mM $MgCl_2$, 1 mM ATP, 100 μg/ml BSA, and 300 ng supercoiled pRYG plasmid DNA, with a titration of the indicated drug from 10 to 250 nM. 120 ng/μl of $hTop2^{FL-\Delta CTD}$ was added to start the reaction. The reaction was terminated by the addition of 0.4 μl of 0.5% SDS and 0.8 μl of 250 mM EDTA and incubated at 37 ºC for 1 hour. Samples were mixed agarose loading dye, and then loading to electrophoresis using 1% agarose gel. DNA band were visualized by UV light.

Topoisomerase DNA Cleavage Assay

The DNA cleavage reaction (20 μl) was conducted at 37 ºC for 30 minutes in a buffer composed of 1 mM ATP, 100 μg/ml BSA, 250 ng of *Hind*III-linearized pRYG plasmid

26

DNA, 20 nM of indicated drug and 1.2 μg/μl of hTop2$^{FL-\Delta CTD}$. The cleavage reaction was

terminated by the addition of 2 μl of 5% SDS followed by 2 μl of 250 mM EDTA. The

enzyme was digested by the addition of 2 μl proteinase K (0.8 mg/ml) and incubation at

45 °C for 30 minutes. For reactions aiming to test the reversibility of DNA cleavage by

the enzymes, EDTA was added to the reactions prior to adding SDS at the termination

step. The resultant reaction mixtures from both assays were resolved by electrophoresis

on a 1% agarose gel followed by standard EtBr staining analysis.

Electrophoretic band shift Assay

The electrophoretic band shift reaction mixture contained assay buffer 35 mM

HEPES pH 7.5, 600 nM 30 bp double-strand DNA, 600 nM hTop2$^{FL-\Delta CTD}$ and add ddH$_2$O

to the final reaction volume 20 μl, then incubated at at 37 °C for 30 minutes. The enzyme-

DNA cleavage complex in the reaction were trapped by the addition of 2 μl of 1.3% SDS,

and sample were incubated at 37 °C for 1 hours. Samples were mixed agarose loading

dye, and then loading to electrophoresis using 6% polyacrylamide gel. DNA band were

visualized by UV light. To determine whether DNA band shift was protein-linked,

proteinase K treatment was added.

ICP-MS (Inductively coupled plasma mass spectrometry)

27

To measure the release of etoplatin-N2α and -N2β from the Top2 cleavage complex, we employed inductively coupled plasma mass spectrometry (ICP-MS) (64), a superior technique for quantitative and ultrasensitive elemental analysis, to detect the platinum signal from the released drugs. The drug-stabilized Top2cc (in a 20 μl reaction) was prepared in a buffer containing 1 mM ATP, 100 μg/ml BSA, 1 μM of a 30 bp double-stranded DNA, 0.5 μM etoplatin-N2α or -N2β and 1.2 μM of hTop2$\alpha^{FL-\Delta CTD}$. After incubating the mixture at 37 ºC for 30 minutes, guanidine hydrochloride (GdnHCl) was added to a final concentration of 1.2 M. Aliquots (10 μl) were sampled at different time points and then diluted with ddH$_2$O to a volume of 100 μl. The sample was then filtered using a 10 kDa-cutoff filter membrane (UFC501096, Amicon Ultra 0.5 mL centrifugal filter) to separate the released (and thus membrane-permeable) drug from those that remained associated with Top2cc. 20 μl of flow-through containing the released drugs was diluted again with ddH$_2$O to a final volume of 3 ml. The resultant sample was then subjected to platinum content determination with an Agilent 7700x ICP-MS in the instrument center of National Taiwan University.

28

3. Results and Discussion

3.1. The structure of hTop2α^{core}-DNA-VM26 ternary complex

Previous studies provide strong evidences that targeting Top2α is sufficient for killing cancer cells. However, no structural information for the drug-stabilized Top2α cleavage complex is currently available. Thus, we followed the approach described in the previous paper (53, 54) and used the co-crystallization and the post-crystallization drug soaking replacement method to resolve the protein-DNA-drug complex. The full-length human hTop2α contains 1531 amino acids (170 kDa). The aim of this study is to investigate the interaction between Top2 poison and Top2 cleavage core, so we truncate the N-gate (ATPase and transducer domains) and remove the unstructured Top2's CTR. The resultant human hTop2α^{core} (termed hTop2α^{core}, residues 436-1188, about 90 kDa) contains the TOPRIM, WHD, Tower domain, and the C-gate (**Figure 1**). Because, the crystals of hTop2α^{core}-DNA-VM26 ternary complex obtained from co-crystallization method diffracted to low resolution and the structural information deduced for the drug binding cleavage core suffered from the lack of atomic details, we use the drug soaking replacement method to get a higher resolution crystal. The hTop2α^{core}-DNA-MIX ternary complex were first transferred to a drug-free stabilization buffer to release the bound MIX, and then transferred the drug-free crystal into a solution that contained the VM26. Using this approach, we successfully prepared crystals of hTop2α^{core}-DNA-VM26 ternary complex that diffracted to higher resolution. These crystals then were subjected into data

30

collection and structure determination processes. The structure is solve by molecular replacement with the PHENIX and undergo rounds of manual model rebuilding and refinement with Coot and PHENIX.
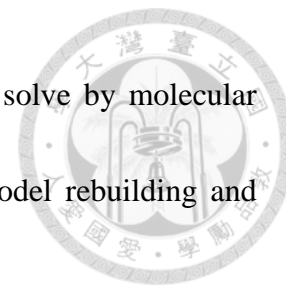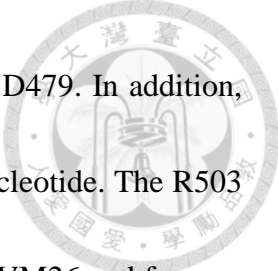
The structure of hTop2α^{core}-DNA-VM26 showed that DNA is bound within a groove formed by the Toprim, WHD, and Tower domains (**Figure 1**). The presence of catalytic Mg^{2+} and VM26 can be recognized in the electron density maps (**Figure 2**). The active site tyrosine forms a transient phosphotyrosyl bond with the +1 nucleotide of DNA, which validates the formation of VM26-induced hTop2α^{core} cleavage complex. The binding of VM26 at the DNA cleavage site effectively prevents the cleaved DNA ends from rejoining (**Figure 2**). A closer look at the VM26 binding mode revealed the drug's tetracyclic aromatic core inserts into cleavage site and stacks with flanking DNA bases. Due to the insertion of drug, the 3'-hydroxyl group (of the -1 nucleotide) is kept away from the enzyme-bridged 5'-phosphate (of the +1 site) by about 8 Å. The VM26 E-ring points toward the DNA minor groove and forms hydrogen bonds with DNA +1, +2 nucleotide and D463 residue. Because the E-ring interacts with both protein and DNA, this branching moiety contributes significantly to the stability of cleavage complex (**Figure 3A**). Residue R487 on the conserved PLRGK loop caps and locks the bound VM26 in the cleavage site. The glycosidic group of VM26 faces the DNA major groove, forming hydrogen bonds with DNA -1 and +5 nucleotide (**Figure 3B**). The sulfur atom of the

thiofuran moiety is about 5.3 Å from residue S800 (corresponds to A816 in hTop2β). It

has been suggested previously that the divergence at this position between hTop2α and

hTop2β might be exploited for developing isoform-specific targeting strategy (54). A

chemical moiety that is longer or bulkier than the glycosidic group would be required to

reach this site.

3.2. Comparison between hTop2α^{core}-DNA-VM26 and hTop2β^{core}-DNA-VM26

The structure of hTop2β^{core}-DNA-VM26 complex were determined by Dr. Chyuan-

Chuan Wu using the drug replacement soaking method mentioned above. Similarly, the

hTop2β^{core}-DNA-EVP ternary complex were first transferred to a drug-free stabilization

buffer to release the bound EVP molecules from these crystals. The VM26 were then

introduced by placing the pre-soaked crystals in a solution that contained the VM26 to

produce new drug-stabilized hTop2β cleavage complex crystal. These crystals were then

subjected to data collection and structural determination process, both DNA and VM26

can be identified in the resultant electron density map (**Figure 4**). We chose to

superimpose on the TOPRIM and WHD domains of hTop2α^{core}-DNA-VM26 and

hTop2β^{core}-DNA-VM26 due to their dominant roles in mediating DNA binding and

cleavage. This comparison revealed no significant changes, all residues around the active

site are well-aligned (**Figure 5A**). Similar to hTop2α^{core}-DNA-VM26, the VM26 E-ring

32

points toward the DNA minor groove, forming hydrogen bond with D479. In addition, the E-ring forms hydrogen bond with main chain of G478 and +2 nucleotide. The R503 on the conserved PLRGK loop acts as a lid to cover the intercalated VM26 and forms a hydrogen bond with A-ring. The non-planar tetracyclic core mediates hydrophobic interactions with DNA to bind stability in the cleavage site (**Figure 5A**). In the DNA major groove, the VM26 glycosidic group forms hydrogen bond with DNA -1 and +5 nucleotides (**Figure 5B**), and a small rotation of the thiofuran moiety was detected. Overall, there are four pairs of diverged residues (M762/Q778、S763/A779、I769/V785 and S800/A816 (α/β)) around the active site. No interactions between M762/Q778 and the glycosidic group of VM26 were observed. The S763/A779 is located on opposite side of the recognition helix with respect to the glycosidic group, and does not contact the bound drug. While the I769/V785 and S800/A816 pairs do not interact directly with the thiofuran moiety, the I769 of hTop2α is slightly bulkier than V785 of hTop2β, thus the DNA-contacting surface of hTop2α is shallower compared to hTop2β (**Figure 6**). This shallower pocket may interact with thiofuran more effectively, consistent with the finding that VM26 has a lower IC50 toward hTop2α than hTop2β (65). This result also agrees with the findings of Shapiro et al. (65) who observed VM26 has better binding affinity to hTop2α. Therefore, to interact more specifically with hTop2α, a smaller hydrophobic group with a properly introduced polar atom would interact with both I769 and S800. In

33

contrast, specific targeting of hTop2β will require a bulkier and more hydrophobic group.

3.3. Structural analysis of hTop2α in complexes with other Top2-targeting agents (Epipodophyllotoxins、Anthraquinone)

To understand how hTop2α interacts with other Top2-targeting agents, we also determined the structures of hTop2α^{core}-DNA-EVP and The hTop2α^{core}-DNA-MIX. Superimposition of hTop2α^{core}-DNA-EVP and hTop2β^{core}-DNA-EVP revealed high degree of similarity between the two structures (**Figure 7**). Notably, while the Q778 of hTop2β forms a hydrogen bond with the glycosidic group via its side chain amide, the side chain of structurally equivalent M762 of hTop2α points at the opposite direction, suggesting that the drug may interact more strongly with hTop2β. However, it was found that EVP binds hTop2α with a slightly lower IC50 than hTop2β (65), the molecular basis of this discrepancy remains to be further explored.

We also compared the structural differences between hTop2α^{core}-DNA-EVP and hTop2α^{core}-DNA-VM26 (**Figure 8**). In the DNA major groove side (**Figure 8B**), a small displacement can be recognized between the two glycosidic groups. It is interesting to note that the VM26 thiofuran is capable of engaging in more extensive hydrophobic interaction with the surrounding protein residues, which explains why the VM26 glycosidic group is positioned closer to protein α-helix compared to that of EVP. This

observation supports the previous finding that VM26 exhibits lower IC50 toward hTop2α

than EVP. Moreover, it can be deduced that the potency of a Top2-targeting agent may be

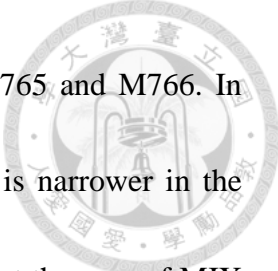adjusted by modifying the major groove-protruding group of the drug.
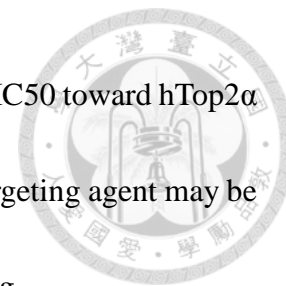
The structure of hTop2α^{core}-DNA-MIX was determined by co-crystallization, in

contrast, the structure of hTop2β^{core}-DNA-MIX obtained from drug soaking replacement

method (54). Despite this difference, the two MIX molecules align well and bind at the

same position (**Figure 22**). This finding demonstrates that the drug soaking replacement

method should be a valid and convenient shortcut for resolving the crystal structures of

drug-protein complexes. In the hTop2α^{core}-DNA-MIX ternary complex, one of the

alkylamino arms extends toward the DNA minor groove forming hydrogen bonds with

N503、E506 and DNA +5 nucleotide (**Figure 9A**). In addition, the residue R487 main

chain forms hydrogen bond with MIX tricyclic aromatic ring. The other alkylamino arm

extends toward the DNA major groove without mediating any interaction. The observed

drug binding mode is quite similar to that of hTop2β^{core}-DNA-MIX (**Figure 9B**). However,

the major groove-protruding arm forms hydrogen bond with Q778 of hTop2β, provide

more interaction than hTop2α, consistent with the finding that MIX exhibits lower IC50

toward hTop2β than hTop2α. Therefore, the small difference observed between

hTop2α^{core}-DNA-MIX and hTop2β^{core}-DNA-MIX bears a direct functional relevance.

This results once again shows that modification of the major groove-protruding moiety

35

may fine tune drug potency.

3.4. Rational for developing isoform-specific Top2-targeting agents

Given the therapeutic side effects caused by the targeting of hTop2β, it is clinically

desirable to develop hTop2α-specific targeting agents. To facilitate drug design, the

structures of hTop2α^{core}-DNA-VM26 and hTop2α^{core}-DNA-MIX were superimposed for

comparison. The DNA-intercalating moiety of Epipodophyllotoxins and Anthraquinones

corresponds to the tetracyclic and tricyclic core, respectively. Due to the structural

difference between their DNA-intercalating moieties, conformational changes were

observed for the +1, -1, +4, and +5 nucleotides. Thus, the cleavage core allow tetracyclic

and tricyclic aromatic ring core insertion and provide stable hydrophobic interaction with

DNA, and it only need to twist the +1、-1、+4 and +5 nucleotides. The conserved PLRGK

loop around DNA minor groove also adopts different conformation in response to the

binding of structurally distinct drugs. Moreover, the R487 functions as a lid to cover and

hold the bound drug in the cleavage site. The side chain of residue M762 in the DNA

major groove changes rotamer according to the substituent size (**Figure 10**). The surface

representation of shows the drug binding site, corresponding to the space enclosed by

DNA +4, +5, +1 and -1 nucleotides, is wider when VM26 is bound (**Figure 11A**). The E-

ring, bulky group push PLRGK loop slightly away from cleavage site. The glycosidic
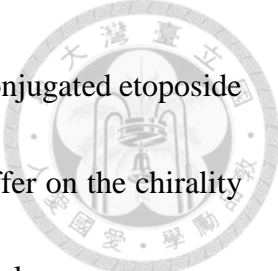
36

group contributes hydrophobic interaction by contacting M762、M765 and M766. In contrast, the space between DNA +4、+5、+1 and -1 nucleotides is narrower in the presence of MIX (**Figure 11B**). This may be explained by the fact that the core of MIX is a planar tricyclic aromatic ring, but the tetracyclic core of VM26 is non-planar. Nevertheless, both the tricyclic or tetracyclic core can be accommodated within the cleavage site to stack with DNA bases upon small adjustment of the +4、+5、+1 and -1 nucleotides. In the Figure 11B, the two alkylamino arms of MIX extend to minor and major groove, respectively. There are more protein residues surrounding the minor groove side for mediating protein-drug interaction, the PLRGK loop moves closer to protein-DNA interface in the MIX-bound structure than VM26. The drug-specific reposition of PLRGK loop not only was observe in hTop2α but can also be detected in hTop2β. However, the amino acids near DNA minor groove are highly conserved between hTop2α and hTop2β. Therefore, interactions mediated via this area would not be useful for achieving isoform-specific targeting. Interestingly, the divergent M762/Q778 pair may be exploited for their differences in polarity and chemical reactivity. Importantly, this position is located at the DNA major groove side, which offers a wider space for design the variant drugs substituent group. Together with the structural information obtained previously on hTop2β (54) led us to propose a set of drug design guidelines. 1. A polycyclic core to facilitate DNA intercalation. 2. A branching moiety that fits between

37

protein and DNA minor groove for enhanced stability and specificity toward the cleavage site. 3. A branching moiety that protrudes toward DNA major groove for mediating isoform-specific interactions.

3.5. Structure-based design of a hTop2-targeting organoplatinum compound

The anticancer drug etoposide is an ideal candidate for testing this concept due to the well comprehended structure-activity relationships regarding its three constituting moieties. The tetracyclic aglycone core composed of rings A~D mediates DNA intercalation and the appended E-ring provides specific interactions with protein residues located on the DNA minor groove side; both moieties are required for optimal drug action and sensitive to modifications (54). Conversely, the pocket that houses the glycosidic group on the DNA major groove side not only is spacious enough to accommodate structurally distinct chemical groups, but also harbors potentially Pt^{2+}-reactive methionine residue(s) (54). Replacing the glycosidic moiety by a Pt^{2+}-containing group may thus allow the formation of Pt^{2+}-thioether bond between the drug and hTop2 isoforms. A diammine linker has already been used successfully to introduce Pt^{2+} into podophyllotoxin (66). Our modeling analysis suggested that adjusting the length of the reported linker should place the Pt^{2+} within a favorable distance for conjugating to a nearby methionine and confers the resulting compounds potent Top2-poisoning activity.

38

We propose to name these compounds etoplatins, representing Pt^{2+}-conjugated etoposide derivatives. Two first generation etoplatins, N2β and N2α, which differ on the chirality by which the diammine linker attaches to the C4 position of the aglycone core were designed and synthesized (**Figure 12**). The synthesis of etoplatin-N2α and N2β (**5β** and **5α,** respectively) started with the preparation of the platinum(II)-diamino-carboxylic acid complex **2** followed by the amide bond formation with 4-amino-4-deoxy-4'-*O*-demethylpodophyllotoxin (**4**). The platinum(II)-4,5-diaminovaleric acid complex (PtCl₂(*N*,*N*-Dav), **2**) was obtained from the reaction of potassium tetrachloroplatinate(II) with 4,5-diaminovaleric acid **1** (67). The (*4S*)- and (*4R*)-4-amino-4-deoxy-4'-*O*-demethylpodophyllotoxins (**4β** and **4α**, respectively) were prepared from 4'-*O*-demethyl-4-*epi*-podophyllotoxin **3** according to literature procedure (68). Subsequently, the amide bond formation between PtCl₂(*N*,*N*-Dav) **2** and 4-amino-4-deoxy-4'-demethylpodophyllotoxins (**4β** and **4α**, respectively) was accomplished by the reaction with *N*-ethyl-*N'*-(3-dimethylaminopropyl)carbodiimide hydrochloride (EDC) and 1-hydroxybenzotriazole (HOBt) in *N*,*N*-dimethylformamide (DMF) to produce etoplatin-N2β and N2α.

3.6. Etoplatin-N2β potently inhibits the supercoil relaxation activity of human Top2 isoforms

39

To examine the effects of etoplatins on the catalytic functions of Top2, we first compared the potency of these platinum organometallic compounds in blocking the Top2-mediated DNA relaxation to that of etoposide (**Figure 13A and 14**). While etoplatin-N2α and etoposide displayed similar inhibitory activities, a 25-fold lower concentration of etoplatin-N2β is sufficient to produce a comparable effect, indicating that etoplatin-N2β is significantly more effective in inhibiting the relaxation activity of both hTop2α and hTop2β. Given that etoplatin-N2β is produced by replacing the glycosidic moiety of etoposide with a thioether-directed, Pt^{2+}-containing reactive center (**Figure 12**), and that both human Top2 isoforms exhibited increased sensitivity towards etoplatin-N2β, we reasoned that the Pt^{2+} center of etoplatin-N2β most likely forms a coordinate bond with the side-chain thioether moiety of Met766 in hTop2α and the spatially equivalent Met782 in hTop2β. In contrast, the N2α enantiomer appears to lack the capacity to form coordinate bond with Top2, and like etoposide, it stabilizes the Top2cc mainly by non-covalent interactions. Together, these results implicate that the formation of a Pt^{2+}-thioether coordinate bond is sensitive to the chirality by which the diammine linker attaches to the aglycone core of etoposide. And the enhanced inhibition activity of etoplatin-N2β may be attributed to the existence of a coordinate bond in the resulting drug-arrested Top2cc.

3.7. The Top2-mediated DNA breaks arrested by etoplatin-N2β are practically irreversible
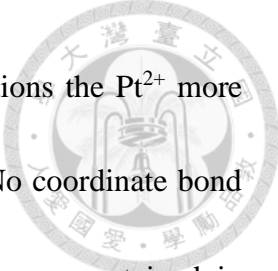
The Top2-mediated double-strand DNA breaks formed in the presence of clinically active hTop2-targeting anticancer drugs are inherently reversible; the two enzyme-tethered, complementary cohesive DNA ends harbored in a Top2cc can be rejoined under conditions where the reversal of transesterification reaction is favored (69-72). For example, exposing the drug-stabilized Top2cc to the Mg^{2+} chelator EDTA before the Top2 activity is permanently blocked by the sequentially addition of protein denaturant and protease is known to promote DNA religation and efficiently restores the integrity of the fragmented DNA, a commonly technique for assessing the reversibility of Top2cc. The speculation that a Pt^{2+}-thioether coordinate bond is formed between etoplatin-N2β and Top2 predicts an enhanced stability of the resulting cleavage complex, presumably less reversible and thus more resistant to EDTA treatment. Indeed, while the DNA breaks induced by etoposide can be readily reversed by pre-treating the cleavage complex with EDTA, as indicated by the disappearance of the smeared DNA fragments and restoration of full-length linear substrate DNA, the breakage resulted from etoplatin-N2β-mediated hTop2 poisoning cannot be resealed (**Figure 13B**). Conversely, the N2α enantiomer appears to lack the capacity to form coordinate bond with either human Top2, and like etoposide, it stabilizes the Top2cc mainly by non-covalent interactions (**Figure 13B**). The

41

production of irreversible, EDTA-resistant DNA breaks by etoplatin-N2β is consistent

with its increased potency and provides additional support for its function as a coordinate
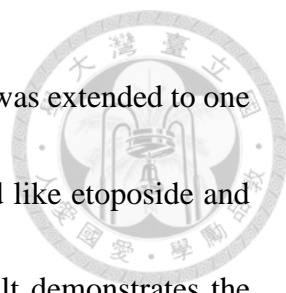
bond-forming inhibitor.

3.8. Crystallographic analysis of human Top2 isoforms in complexes with DNA and etoplatins

To confirm the proposed mechanisms of action for etoplatins, we performed X-ray

crystallographic analysis on the etoplatin-stabilized cleavage complexes of hTop2β.

Similar to etoposide, both etoplatins trap the Top2cc by targeting the enzyme-mediated

DNA breaks, with the aglycone core intercalating between the base pairs flanking the

cleavage site and the E-ring protruding towards the DNA minor groove to interact with

surrounding residues (**Figure 15B and C**). As expected, the diammine linker extends

towards the DNA major groove side and places the reactive dichloroplatinum(II) moiety

in the general vicinity of the methionine residue(s) located in helix α4 of the Top2

winged-helix domain. For etoplatin-N2β, one of the chloride ions is replaced by the

methionyl S^{δ} of M782 in hTop2α (M766 in hTop2β) with clear electron density

connecting S^{δ} and Pt^{2+}, indicating a coordinate bond with a refined bond length of 2.3Å

is formed (**Figure 15A and 16A**). Due to the structural constraints imposed by the

alternative stereochemistry at the C4 chiral center, the dichloroplatinum(II) moiety of

42

etoplatin-N2α is directed closer to the +1/+4 base pair, which positions the Pt^{2+} more

distantly (~4.3 Å) from the methionyl S^{δ} (**Figure 15C and 16B**). No coordinate bond

formation was observed and both of the Pt^{2+}-ligating chloride ions are retained in

etoplatin-N2α. Although the crystal structures of etoplatin-bound hTop2α are not yet

available, structural modeling analysis predicted that hTop2α would form a coordinate

bond with the bound etoplatin-N2β via the methionyl S^{δ} of M766 (corresponding to M782

in hTop2β) (**Figure 17**). In contrast, etoplatin-N2α would not coordinate with either

M766 or M762 because their S^{δ} are too distant from the coordination sphere of Pt^{2+} to

replace the Cl^{-} ligand (**Figure 17B and 17C**). Together, the results obtained from

crystallographic and modeling analyses provide convincing evidence that etoplatin-N2β

acts as a potent and irreversible poison of human Top2 isoforms through its coordinate
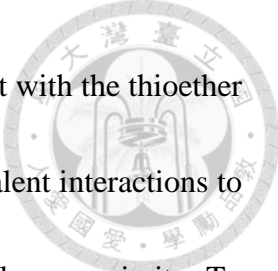
bond forming capability.

We have shown previously that the conventional non-covalent Top2-targeting

drugs can be released from the crystallized Top2 cleavage complex by an overnight

soaking of the respective crystals in a drug-free substitute mother liquor, and that the

binding of a different drug can be achieved by another overnight soaking of these pre-

treated crystals in a solution containing the new drug (54). When subjected to this two-

step soaking procedure with another hTop2-targeting drug mitoxantrone being added in

the second soaking solution, we observed the persistent presence of etoplatin-N2β in the

43

DNA cleavage site even when the length of the second soaking step was extended to one week (**Figure 18**). The bound N2α enantiomer, in contrast, behaved like etoposide and can be efficiently replaced following the same treatment. This result demonstrates the coordinate bond formation confers remarkable stability to the etoplatin-N2β-stabilized Top2 cleavage complex, which in turn contributes to its enhanced Top2-poisoning activity.

3.9. The coordinate tether between etoplatin-N2β and hTop2 exhibits a protein conformation-dependent reversibility
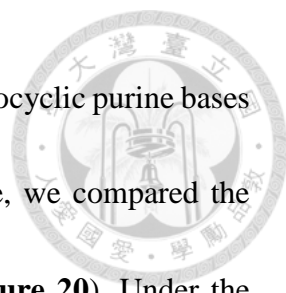
Earlier solution NMR analysis of the methionine-conjugated platinum(II) diammine complexes revealed that the mono-methionine derivative was susceptible to competition by guanosine 5`-monophosphate, as shown by the release of the Pt^{2+}-ligated methionine, whereas the bis-methionine compound was substantially more resistant to ligand replacement and thus displayed greater stability in aqueous solution (73). The presence of only a single Pt^{2+}-thioether linkage between etoplatin-N2β and hTop2 suggests that the resulting tetracoordinate Pt^{2+} center is chemically similar to the more labile mono-methionine compound. Nevertheless, the coordinate bond formed between the cleavage site-bound etoplatin-N2β and hTop2β^{core} exhibited an outstanding stability (**Figure 18**). We speculated that the compound's podophyllotoxin moiety may contribute substantially

44

to the enhanced stability by not only delivering the Pt^{2+} center to react with the thioether

group of M782 in a site-specific manner, but also providing non-covalent interactions to

sustain the Pt^{2+}-thioether bond by keeping the metal/ligand pair in close proximity. To

examine the validity of this hypothesis, we tested whether the bound etoposide-N2β can

dissociate from Top2cc upon guanidine hydrochloride (GdnHCl)-induced protein

denaturation (**Figure 19A**). As expected, an increase in the Pt^{2+} concentration from the

detached etoplatin-N2β, as judged by its ability to pass through an ultrafiltration

membrane (M.W. cutoff: 10 kDa), was observed in the presence of GdnHCl (**Figure 19A**).

In contrary, for the untreated sample, no significant membrane permeable signal of Pt^{2+}

could be detected after 28 hours of incubation at 37ºC. This result supports the importance

of non-covalent interactions in stabilizing the coordinate bond. Moreover, it can be

inferred that the strength of a metal-protein linkage may be reduced upon disruption of

the protein structure. Therefore, the apparently irreversible trapping of Top2cc by

etoplatine-N2β exhibits protein conformation-dependent reversibility.

3.10. Etoplatin-N2β displays reduced reactivity toward DNA compared to cisplatin
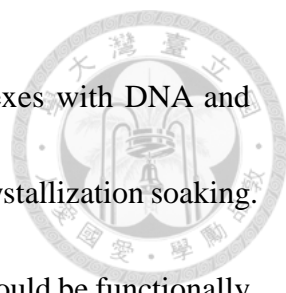
While the aforementioned results establish etoplatin-N2β as a potent hTop2 poison,

the chemical similarity between its reactive cis-diamminedichloridoplatinum (II) moiety

and the anticancer drug cisplatin (cis-diamminedichloridoplatinum(II); cis-$[Pt(NH_3)_2Cl_2]$)

45

raises a possibility that etoplatin-N2β may also react with the N-heterocyclic purine bases

to form intrastrand or interstrand DNA crosslinks   (74). Therefore, we compared the

DNA crosslinking ability of etoplatin-N2β to that of cisplatin (**Figure 20**). Under the

similar experimental condition as used for examining the supercoil relaxation and DNA

cleavage activities of hTop2, essentially all DNA substrates were converted to a slower

migrating form in the presence of 50 μM cisplatin, indicating complete formation of drug-

DNA adduct. In contrast, only a small fraction of the DNA substrates was modified with

the same level of etoplatin-N2β, suggesting the DNA crosslinking activity of the Pt^{2+}

center is significantly reduced, likely due to the steric bulkiness of the attached

podophyllotoxin core. Notably, the addition of hTop2α resulted in a dose-dependent

accumulation of a high molecular weight species that was also observed in the presence

of etoposide (**Figure 20**; lanes 4, 6 and 9). The sensitivity displayed by this species to

proteinase K treatment revealed its identity as the drug-stabilized Top2cc. This result once

again shows the high specificity of etoplatin-N2β toward the Top2-mediated DNA

cleavage site.

4. Conclusion

In this work, we determined structures of hTop2[core] in complexes with DNA and various Top2-targeting agents by co-crystallization as well as post-crystallization soaking. All the structural information obtained are consistent and therefore should be functionally relevant. Therefore, the post-crystallization soaking procedure should be an valid approach if one wishes to characterize the structure of hTop2[core]-DNA-drug in the short time. In addition, there are three pairs of divergent residues (M762/Q778、I769/V785 and S800/A816) in the drug binding pocket, which may be exploited to achieve isoform-specific targeting.

To test this idea, we conducted structure-based modification of the clinically active anticancer drug etoposide to produce an organoplatinum compound (**Figure 12**), etoplatin-N2β, which exhibits potent Top2-poisoning activity (**Figure 13**). The podophyllotoxin core of this new compound offers binding specificity towards the Top2-meidated DNA cleavage site and the appended cis-dichlorodiammineplatinum(II) moiety strengthens drug-protein interaction by forming a Pt^{2+}-thioether coordinate bond with a flanking methionine residue (**Figures 15 and 16**). Our results clearly show that selective targeting of a specific methionine residue in protein can be achieved by exploiting the Pt^{2+} coordination chemistry, and that the combination of a single Pt^{2+}-thioether linkage and non-covalent interactions between the drug and protein is sufficient to increase the stability of the resulting Top2-DNA-drug ternary complex.

It has been well documented that patients receiving Top2-targeting anticancer drugs are at risk of developing therapy-related secondary leukemia and cardiac problems (42, 75, 76). Mounting evidences suggest that the undifferentiated targeting of both human Top2 isoforms by these drugs is likely the main cause of adversity: while poisoning of hTop2α is sufficient for killing cancer cells, the induction of hTop2β-mediated DNA breaks and chromosome translocation events may result in deleterious side effects (77-80). To overcome these problems, it would be clinically desirable to develop a hTop2α-specific drug without simultaneous targeting of hTop2β. Structural analysis of the etoposide-bound hTop2α cleavage complex (**Table 1**) revealed that, compared to the Pt^{2+}-coordinating methionine that was either observed (M782 of hTop2β) or predicted (M766 of hTop2α) in this study, the thioether side chain of the hTop2α-specific methionine (M762) is located significantly closer to ring C of the bound podophyllotoxin core (**Figure 22**). Therefore, we envision a shorter diammine linker with properly designed stereochemistry would deliver the reactive Pt^{2+} center towards M762 to achieve selective targeting of hTop2α over the β-isoform, which instead, possesses a glutamine (Q778) at the corresponding position. We have taken the first step toward this end by designing a series of synthesizable compounds with altered linker structure and length (**Figure 23**). For all these compounds, structural modeling showed that the Pt^{2+} can be placed at ~2.3 Å from the S$^{\delta}$ of M762 to allow coordination bond formation, whereas the

49

simulated distances between Pt^{2+} and the S^δ of M766 are much longer (> 5.0 Å) and thus preclude bond formation between the two. This analysis suggests that selective targeting of hTop2α via the isoform-specific M762 may be an achievable goal.
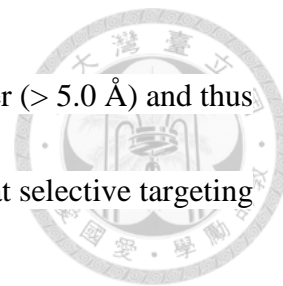
A potential advantage of employing Pt^{2+}-thioether coordination chemistry in drug design is that the stability of the resulting coordinate tether formed between the drug and its target methionine appears to rely on the existence of drug-mediated non-covalent interactions (**Figure 19A**). Damage to the structural integrity of the drug binding pocket by protein denaturant is expected to abolish the non-covalent part of the interactions between drug and Top2cc, the accelerated release of etoplatin-N2β from Top2cc in the presence of GdnHCl indicates the Pt^{2+}-thioether linkage was weakened upon protein unfolding (**Figure 19B**, top panel). Although in this experiment the dissociation of Top2cc-attached etoplatin-N2β is initiated rather artificially by the addition of GdnHCl, we speculate a similar protein unfolding-triggered drug dissociation event may also take place *in vivo*. The repair of double-strand DNA breaks harbored by the drug-arrested Top2cc involves unfolding and 26S proteasome-dependent proteolytic removal of Top2 (40, 81), which would disrupt the non-covalent drug-protein contacts and renders the Pt^{2+}-thioether bond reversible (**Figure 19B**, bottom panel). Unlike covalent inhibitors that usually form irreversible adducts with proteins or nucleic acids, the organoplatinum

50

compounds display a protein conformation-dependent reversibility, and hence may be less toxic and antigenic.

Taken together, our results suggest a general approach for developing organoplatinum compounds that permit targeting of a specific methionine residue in proteins: a successful compound should carry a collection of suitable pharmacophores that are recognized by the target protein via the formation of a non-covalent complex, the dichloroplatinum(II) moiety of the compound would then coordinate with a nearby methionine side chain to further stabilize the drug-protein interaction. This strategy is expected to allow effective targeting of any protein with a methionine-containing drug binding pocket. In addition to the successful development of etoplatin-N2β as a potent hTop2 poison, it appears that bacterial DNA gyrase and a drug-resistant epidermal growth factor receptor (EGFR) variant carrying a T790M mutation would also be ideal candidates for illustrating the applicability of using Pt^{2+}-thioether coordination in drug design. The binding site of Novel Bacterial Type II Topoisomerase Inhibitors (NBTIs) that target bacterial DNA gyrase features the presence of several methionine residues (**Figure 24**) (82); we suspect a Pt^{2+}-derivatized quinolone may overcome drug-resistant mutations by strengthening protein-drug interaction. Similarly, the T790M mutation, located in the EGFR's ATP binding site, weakens the interaction between EGFR and the tyrosine kinase inhibitor gefitinib (83, 84). A Pt^{2+}-derivatized gefitinib with the ability to coordinate with

51

M790 may restore its association with EGFR. In summary, the integration of the dichloroplatinum(II) moiety into an existing drug, as shown in the development of etoplatin-N2β, may represent an effective technical shortcut for boosting the drug's bioactivity.
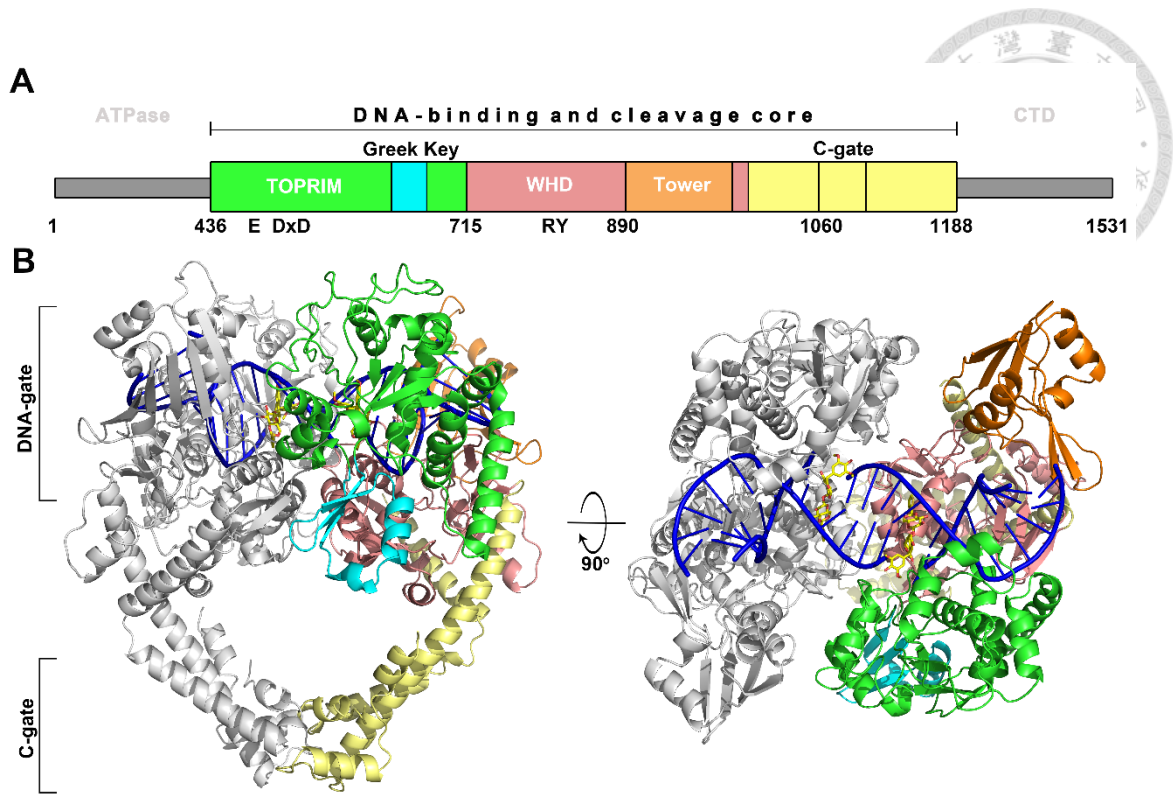
5. Figures

Figure 1. Structure of the VM26-stabilized human Top2α^{core} cleavage complex.

(**A**) The domain organization of human Top2α DNA-binding and cleavage core fragment

(residues 436-1188). (**B**) The structure of ternary cleavage complex. DNA is in blue. The

bound VM26 is shown in yellow sticks representation. One hTop2α^{core} monomer is in

gray and the other is colored following the scheme shown in panel (**A**).
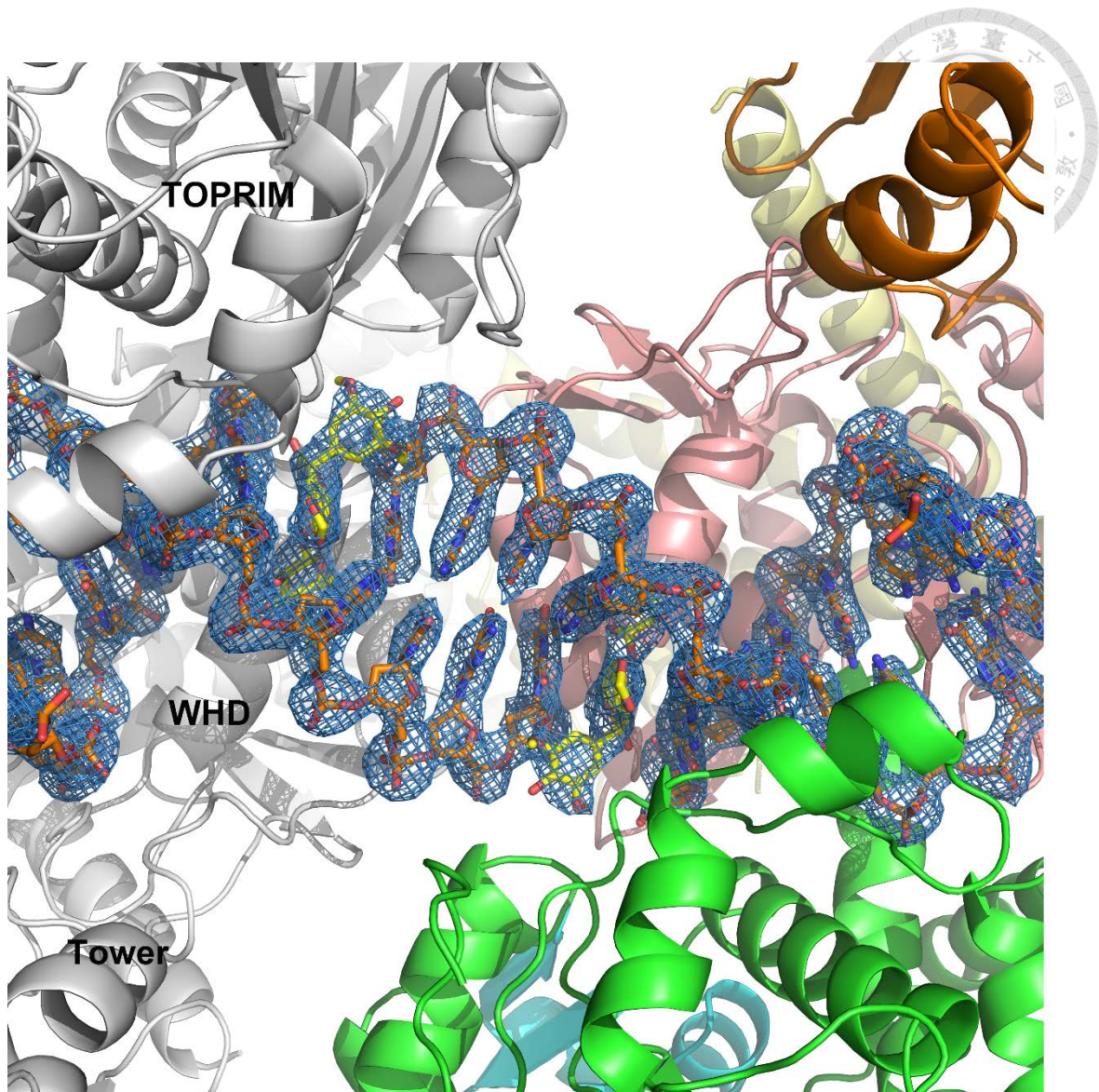
Figure 2. The electron density map of VM26-stabilized human Top2α^{core} cleavage complex.

The 2mF_{o}-DF_{c} electron density maps (contoured at 2σ) of the bound VM26 (yellow sticks) and 20 base pairs DNA duplex (orange sticks) show the insertion of the drug into the two DNA cleavage sites. Protein is colored according to Figure 1A.
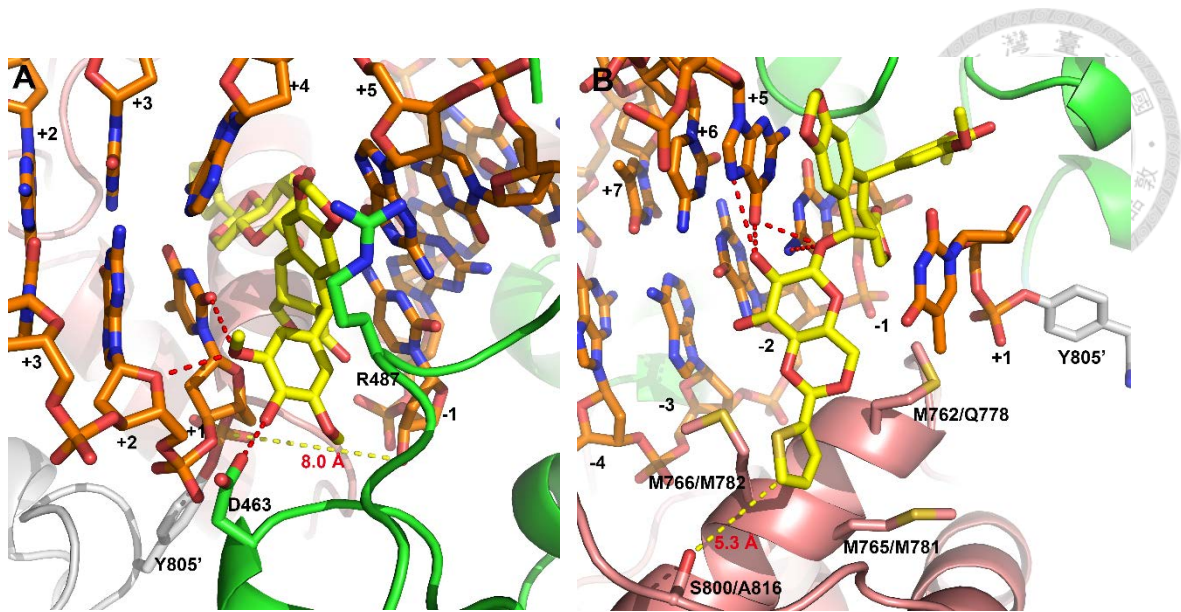
55

Figure 3. Detailed view of the VM26 binding site.

(**A**) Close-up view of the minor groove binding pocket where accommodates the E-ring of VM26. The yellow dotted line shows the distance between active site Y805'-linked scissile phosphate and the 3'-OH. The red dotted lines illustrate hydrogen-bonding. (**B**) Close-up view of the minor groove binding pocket where accommodates the glycosidic group of VM26. The distance between the thiofuran of VM26 and S800 is about 5.3Å. Protein is colored according to Figure 1A.

56
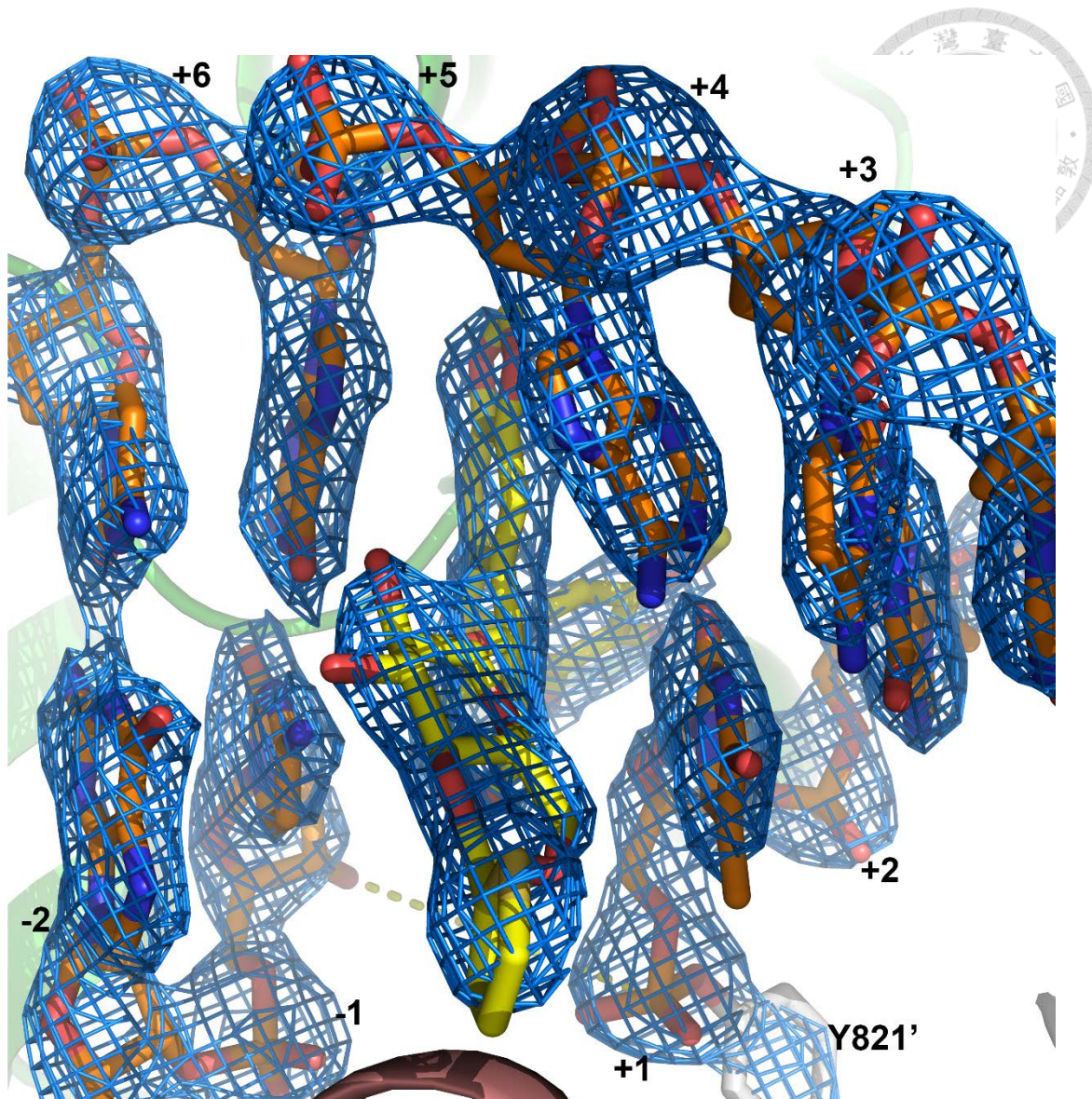
Figure 4. The electron density map of VM26 in the hTop2β^{core}-DNA-VM26

complex structure.

The clear electron density maps of VM26's thiofuran group in the solved structure

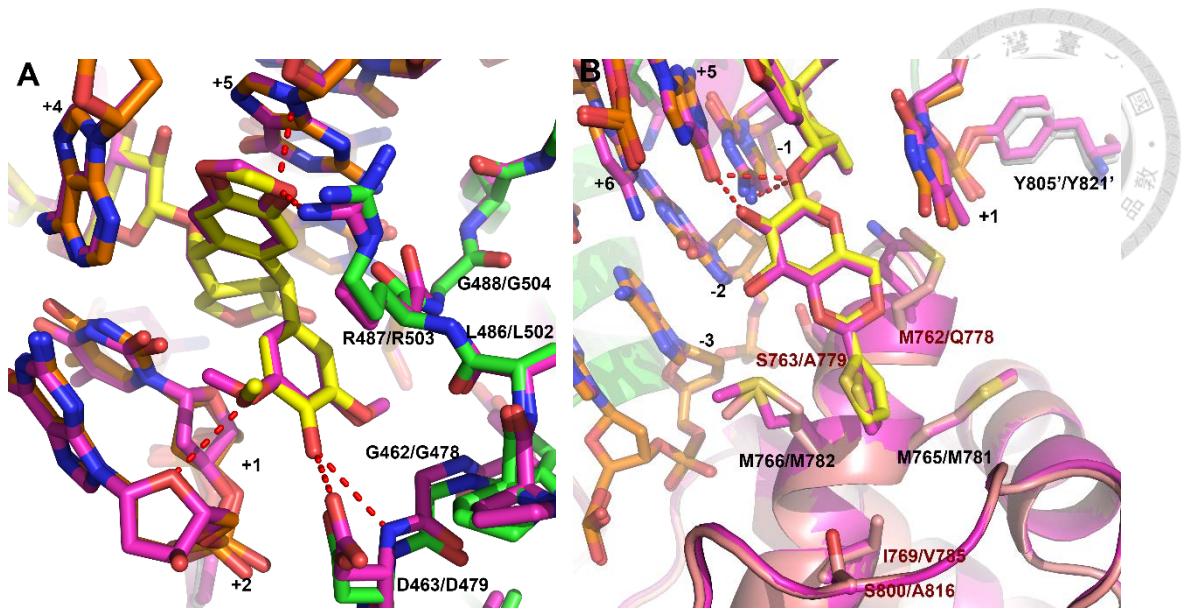indicates etoposide had been successfully replaced by VM26 in the crystal.

Figure 5. Superimposition of hTop2α^{core}-DNA-VM26 and hTop2β^{core}-DNA-VM26.

The detailed view of DNA minor groove (**A**) and major groove (**B**) -drug binding pocket

in the structure. For the both panels, hTop2α^{core} is colored according to Figure 1A, and

hTop2β^{core} is colored in purple.
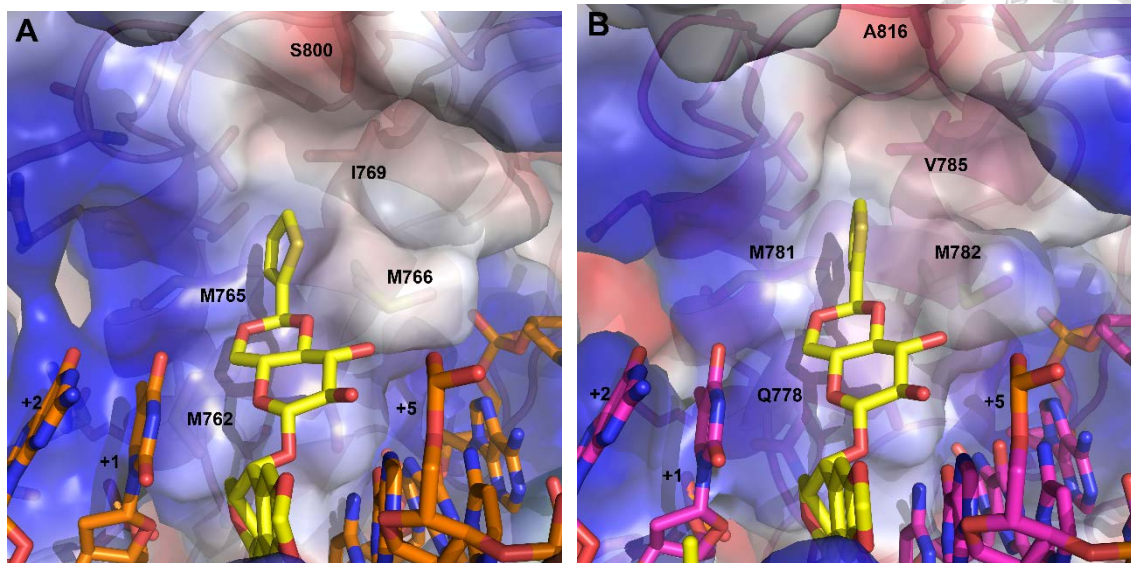
58

Figure 6. Surface representation of DNA minor groove drug binding pocket in the hTop2α^core-DNA-VM26 and hTop2β^core-DNA-VM26 complex structures.

(**A**) Surface representation of DNA minor groove drug binding pocket in the hTop2α^core-DNA-VM26 complex structure. Residues M765、M766 and I769 provide hydrophobic interaction with thiofuran group. (**B**) Surface representation of DNA minor groove drug binding pocket in the hTop2β^core-DNA-VM26 complex structure. Residues M781、M782 and V769 provide hydrophobic interaction with thiofuran group. In the two structures, although the bound VM26 displays similar interaction with the respective proteins, however, we also noticed that residues S800 and I769 in hTop2α and residues A816 and V785 in hTop2β introduce different landscape to the pocket, which might be explored to achieve human Top2 isoform specific drug targeting.
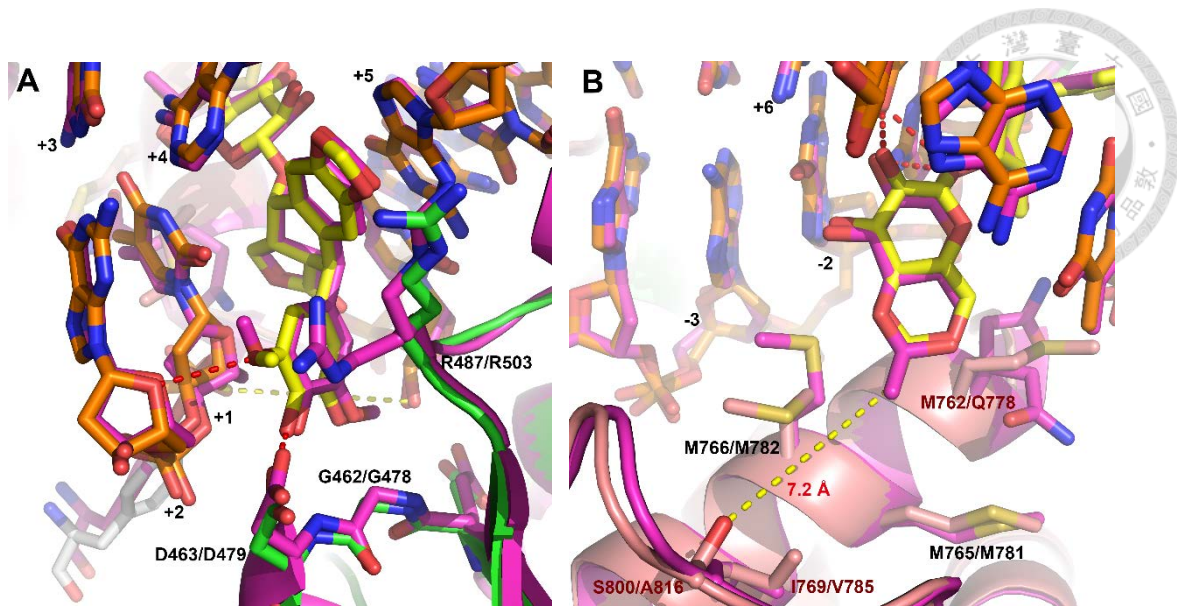
Figure 7. Superimposition of hTop2α^core-DNA-EVP and hTop2β^core-DNA-EVP.

(**A**) The detailed view of EVP E-ring toward DNA minor groove and binding pocket, the dash line show the interaction between drug and hTop2α^core-DNA. The yellow dash shows the distance between Y805'-linked scissile phosphate and the 3'-OH. (**B**) The binding pocket of EVP glycosidic, it shows the similar interaction and drug rotation from hTop2α^core-DNA-EVP and hTop2β^core-DNA-EVP. The hTop2α^core colors present protein domain as same as Figure 1A, and hTop2β^core colors show in purple.

60

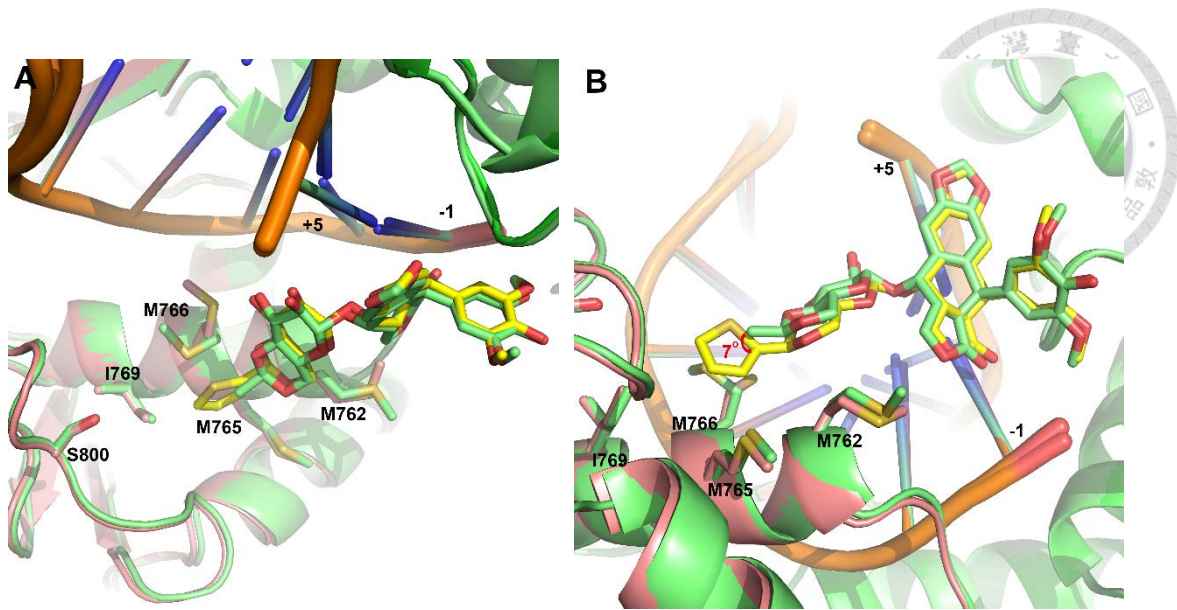**Figure 8. Superimposition of hTop2α^core-DNA-VM26 and hTop2α^core-DNA-EVP.**

(**A**) The drug binding pocket around DNA major groove and α4 helix. The ABCDE ring have similar position between VM26 and EVP. (**B**) The glycosidic ring of EVP have slightly lift about 7°. The hTop2α^core-DNA-VM26 colors present protein domain as same as Figure 1A, and hTop2α^core-DNA-EVP colors show in lime.

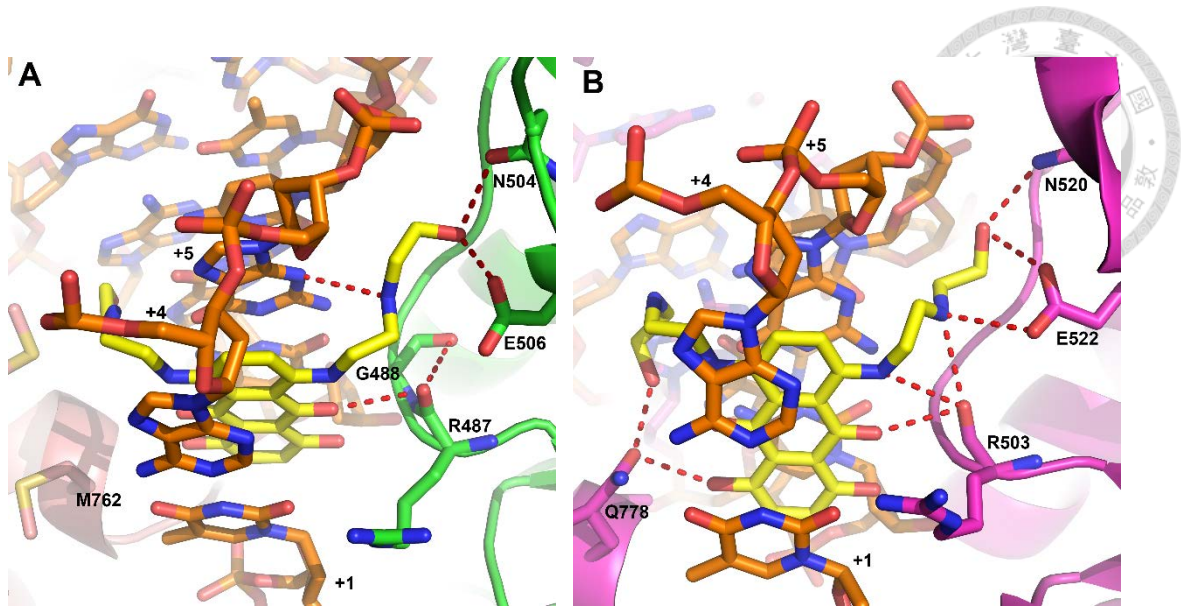**Figure 9. The MIX-stabilized human Top2α^{core} cleavage complex binding pocket.**

(**A**) The pocket of hTop2α^{core}-DNA-MIX. The residues R487、E506 and N504 at DNA minor groove forming hydrogen bond interaction with MIX. (**B**) The pocket of hTop2β^{core}-DNA-MIX. The residues R503、E522 and N520 at DNA minor groove forming hydrogen bond interaction with MIX. Two of these pocket have similar interaction. However, the residue Q778 in hTop2β forming additional interaction with MIX. The hTop2α^{core} colors present protein domain as same as Figure 1A, and hTop2β^{core} colors show in purple.
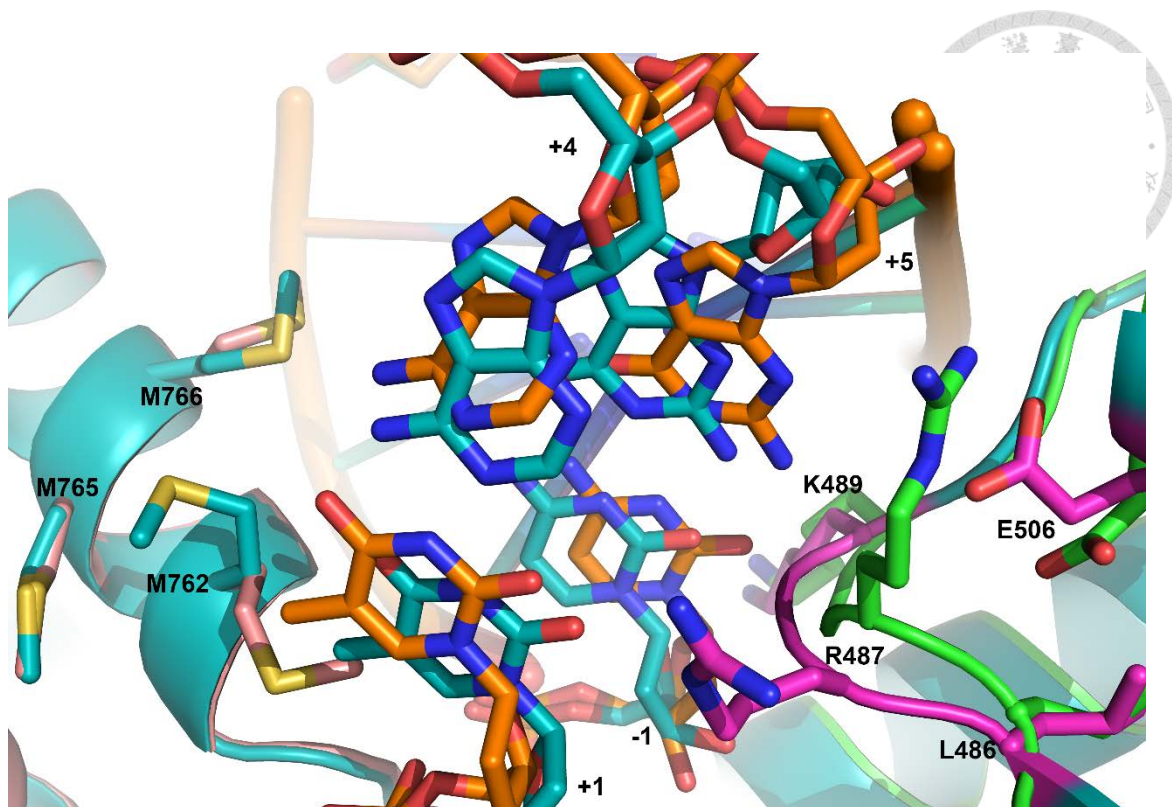
Figure 10. Superimposition of drug binding pocket of hTop2α^core^-DNA-VM26 and hTop2α^core^-DNA-MIX.

The different anticancer drugs binding pocket show the DNA +1、-1、+4、+5 position.

The DNA in the binding pocket have slightly shift, and other have well alignment. The

PLRGK motif show different rotation for fit drug binding. The hTop2α^core^-DNA-VM26

colors present protein domain as same as Figure 1A, The hTop2α^core^-DNA-MIX colors
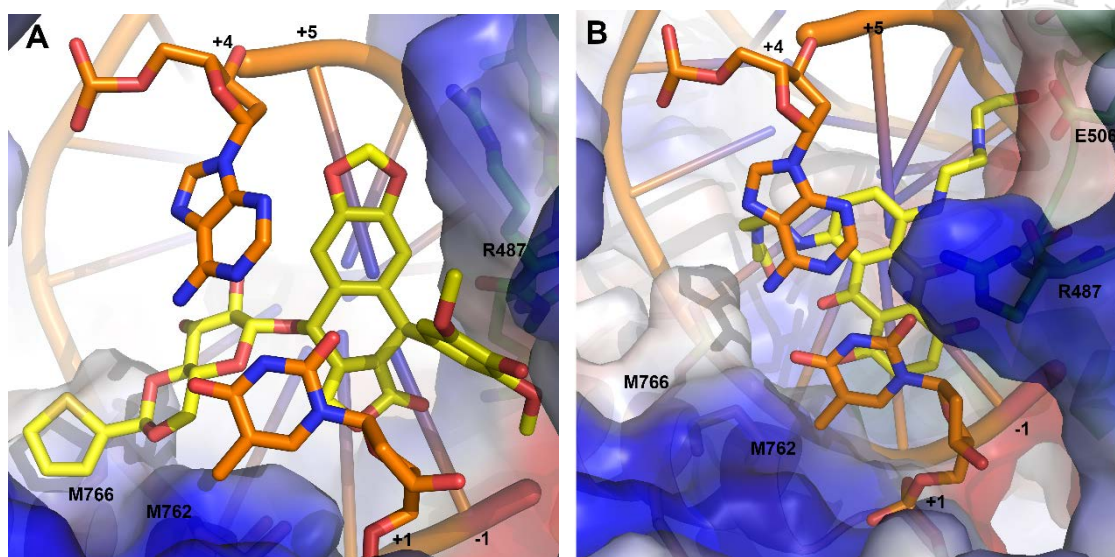
show in limegreen and PLRGK motif show in purple.

Figure 11. The surface views of VM26 and MIX binding pocket.

(**A**) VM26 binding into active site between DNA +4/+1 and +5/-1, the E-ring toward minor groove and glycosidc moiety toward major groove. (**B**) MIX shows the same view of (**A**). Two of them present protein domain colors as same as Figure 1A, and drugs show in yellow. The residue R487, in the binding pocket, has different position between two drugs binding.
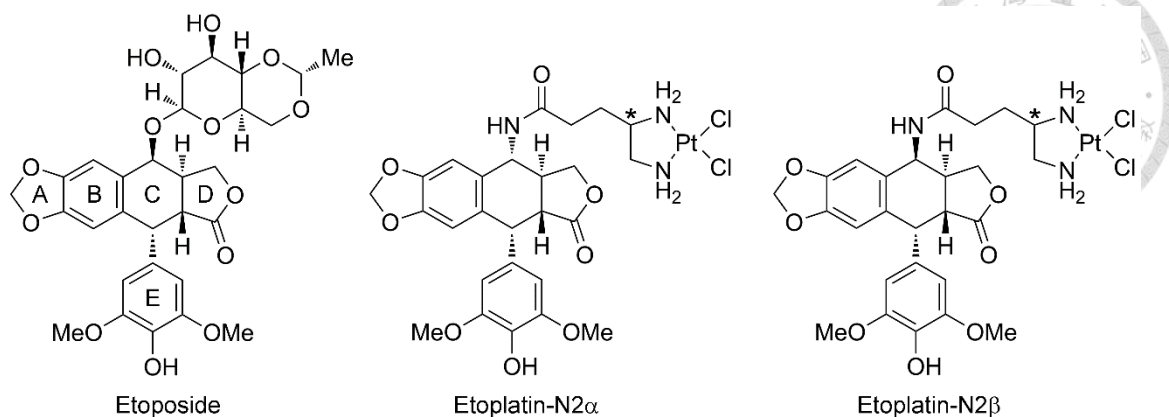
64

Figure 12. Chemical structures of etoposide and the two etoplatins synthesized in this study.

The polycyclic aglycone (rings A–D) and pendant ring (E-ring) of etoposide are labeled.

A cis-dichlorodiammineplatinum(II) moiety was introduced via an amide linkage to the

C4 position of the aglycone core in α and β configuration about the E-ring to produce

etoplatin-N2α and N2β, respectively. Both etoplatins contain an additional chiral center

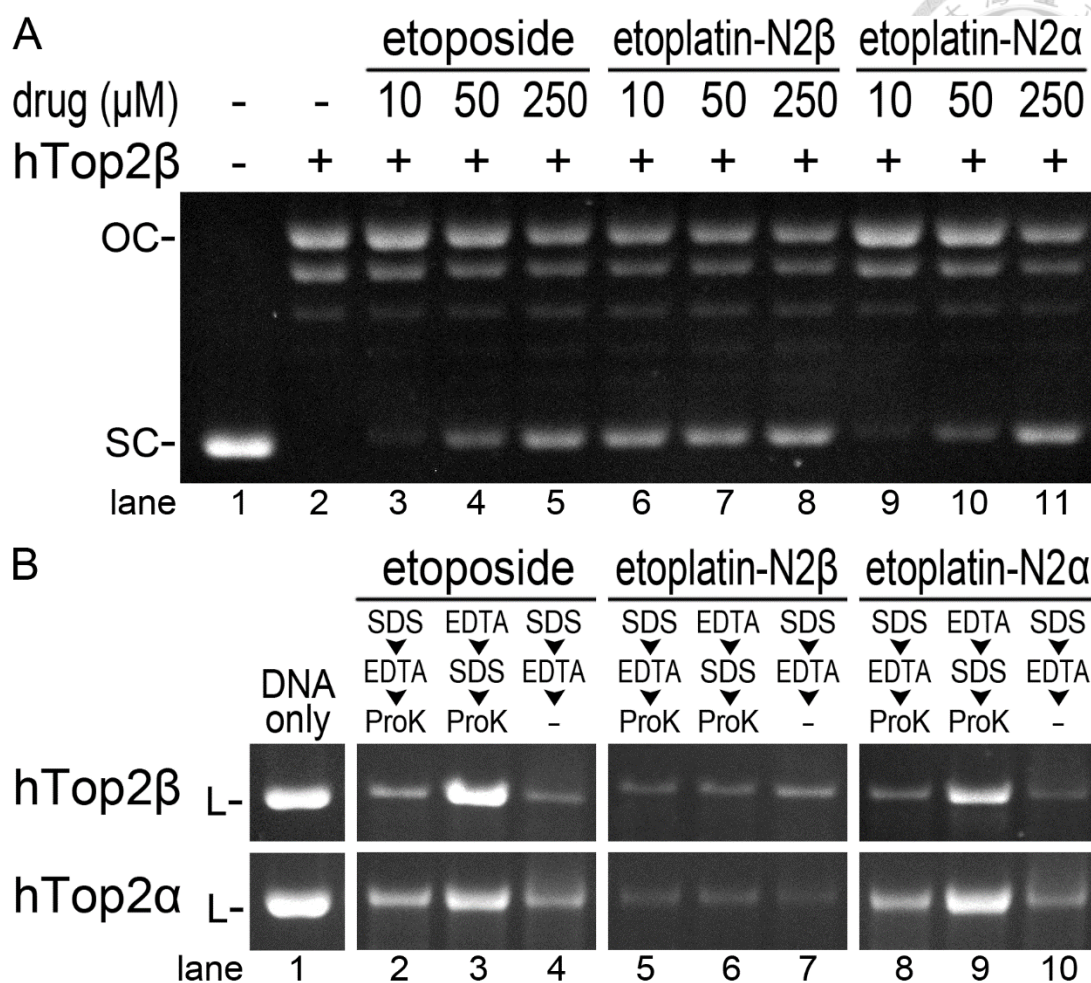(marked with asterisks) whose chirality was not specified during synthesis.

65

Figure 13. Inhibition of the relaxation and cleavage activity by etoposide and etoplatins.

Etoplatin-N2β, but not the N2α enantiomer, more potently inhibits the supercoil relaxation activity of Top2 by inducing the formation of EDTA-resistant DNA breaks. (**A**) Inhibition of the relaxation activity of hTop2 by etoposide and etoplatins. Each relaxation reaction contains 300 ng of supercoiled (SC) pRYG plasmid DNA. The enzyme-positive reactions contain 80 ng of hTop2β. OC stands for open circle (full-relaxed product produced by Top2) DNA. (**B**) The DNA cleavage assay shows the production of EDTA-

resistant, hTop2-mediated DNA breaks in the presence of etoplatin-N2β. Each cleavage reaction contains 250 ng of *Hind*III-linearized (L) pRYG plasmid DNA. 1.2 µg of hTop2β (upper panel) or hTop2α (lower panel) were added to the enzyme-positive reactions, respectively. To stop the cleavage reaction, SDS and EDTA were added in the indicated order, the denatured enzyme was removed by proteinase K digestion. Lanes labeled with -ProK indicates no proteinase K treatment after the reaction was stopped.
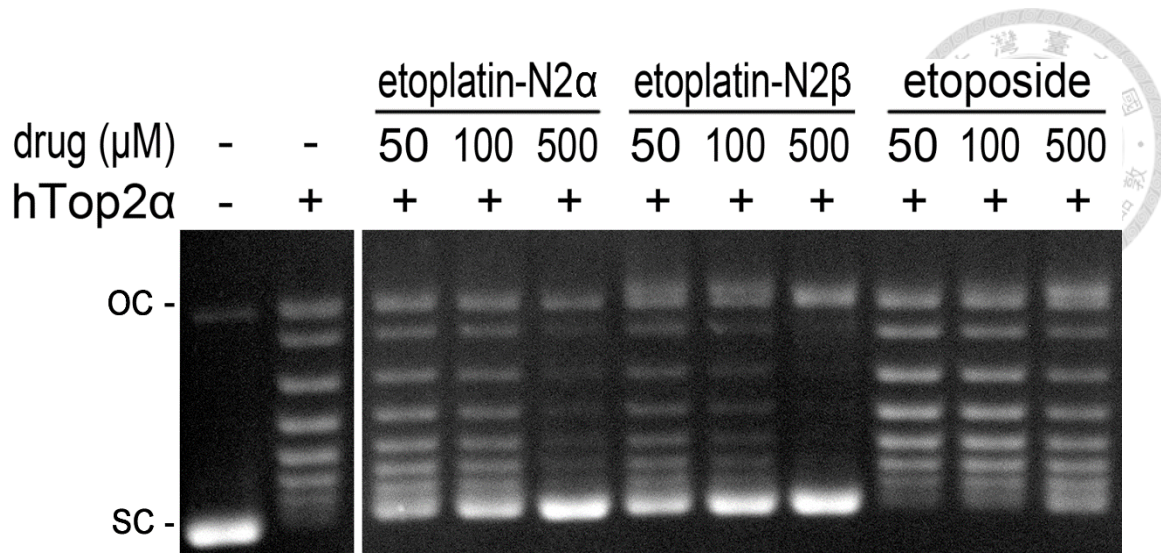
67

Figure 14. Inhibition of the relaxation activity of hTop2α by etoposide and etoplatins.

Each relaxation reaction contains 300 ng of supercoiled (SC) pRYG plasmid DNA. The enzyme-positive reactions contain 120 ng of hTop2α$^{FL-\Delta CTD}$, a fully active proxy for hTop2α. OC stands for open circle (fully-relaxed product produced by Top2) DNA. Similar to the result shown in Figure 13A, etoplatin-N2β, but not the N2α epimer, more potently inhibits the relaxation activity of hTop2α compared to etoposide.
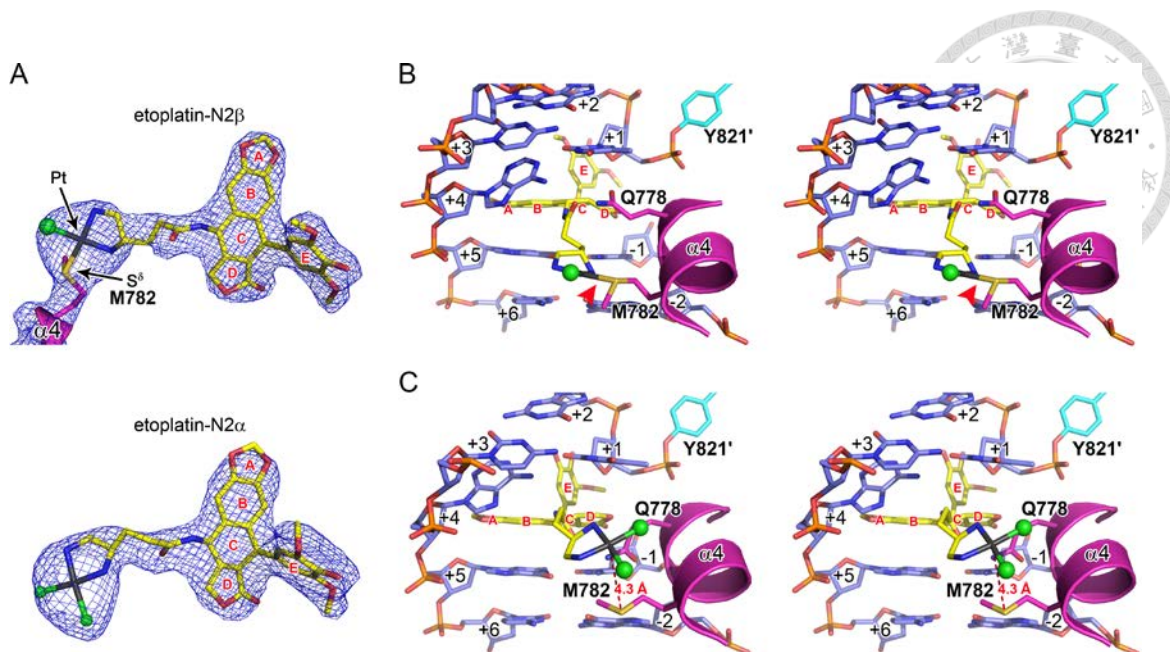
Figure 15. Detailed view of etoplatins binding site.

Both etoplatin-N2β and -N2α bind to the DNA cleavage sites in the hTop2βcc crystal structure as etoposide but only etoplatin-N2β forms the irreversible Pt^{2+}-thioether coordinate bond. (A) The electron density maps of the bound drugs in the crystal structures of hTop2β^{core}-derived cleavage complexes stabilized by etoplatin-N2β (upper panel) and etoplatin-N2α (lower panel). The final $2DF_o$-mF_c maps (at 1.5 σ) of the respective drugs are shown as blue meshes. Continuous electron density can be observed between Pt^{2+} and the $S^δ$ of M782, indicating the formation of a coordinate bond. (B and C) Stereo views of the drug-binding site in the etoplatin-N2β- and etoplatin-N2α-stabilized cleavage complexes derived from hTop2β^{core}, respectively. The Pt^{2+}-thioether coordination in the etoplatin-N2β-stabilized structure in *B* is specified by the red arrow. DNA is shown in sticks representation (blue) and labeled with positive and negative numbers to designate nucleotides downstream and upstream, respectively, of the scissile

69

phosphate. The bound drugs are shown in sticks representation (yellow) with the Pt^{2+} in gray and Cl^- in green spheres. The drug's aromatic rings are labeled in red letters. The two protein chains are shown in a cartoon/stick representation and colored in magenta and cyan, respectively. The scissile phosphate-linked active site Y821 is labeled with a prime to specify that this residue is from the second protein chain.
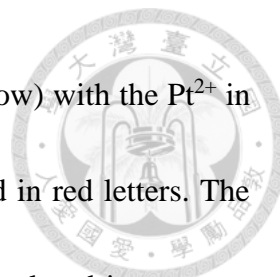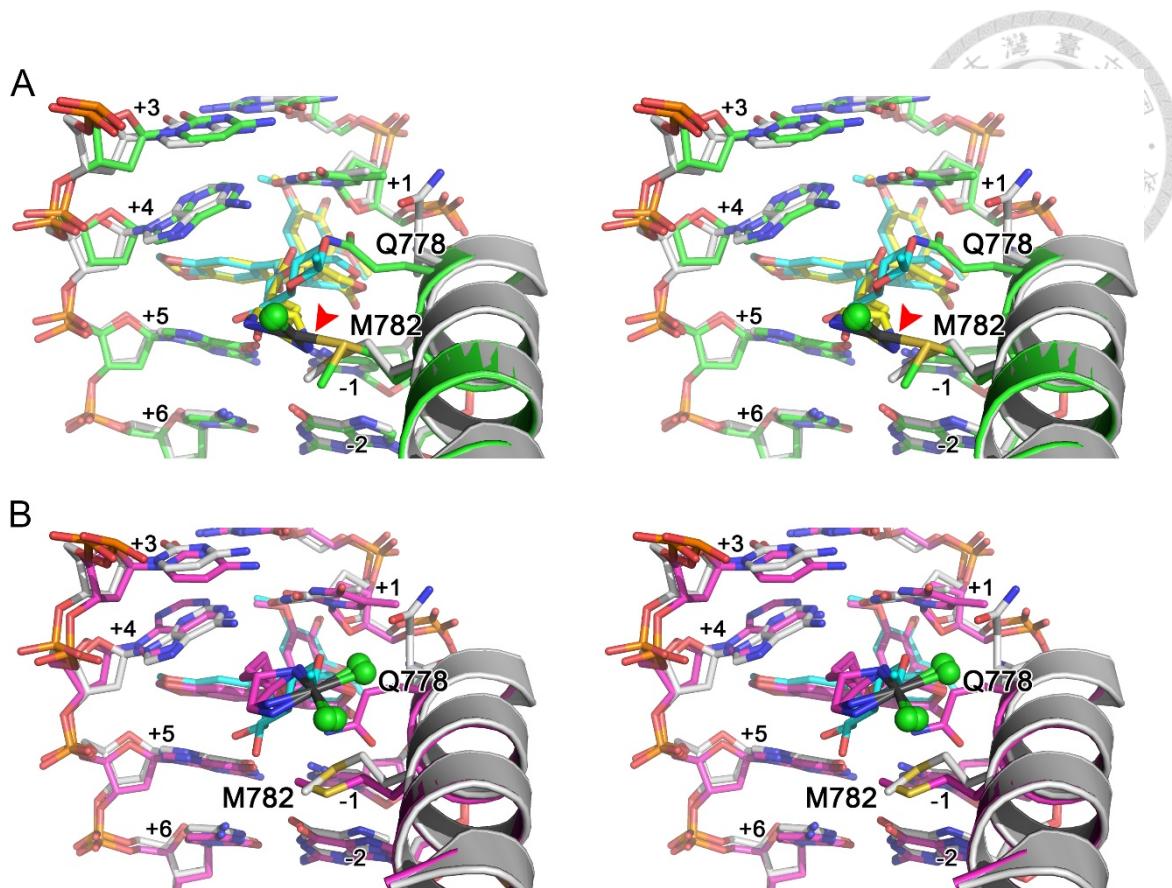
Figure 16. Superimposition of hTop2β-DNA-EVP and hTop2β-DNA-etoplatins.

Structural superimposition of the hTop2β^core-derived cleavage complex stabilized by

etoposide (PDBid: 3QX3, (53)) and the ones stabilized by etoplatin-N2β (A) and -N2α

(B). In both panels, the parental etoposide-bound structure is shown in gray, and the newly

determined structures bound by etoplatin-N2β and -N2α are colored in green and purple,

respectively. The bound etoposide in the parental structure is shown in cyan stick

representation, and etoplatin-N2β and -N2α are in yellow stick representation. Regardless

of the bound drug, the protein parts of these structures are resonably well aligned,

indicating the lack of significant structural changes upon drug replacement. It is

noteworthy that the Q778 and M782 side chains adopt different rotamer conformations

in response to the presence of a stereochemically distinct Pt^{2+}-coordinating diammine

linker of etoplatin-N2α and N2β.

72

A
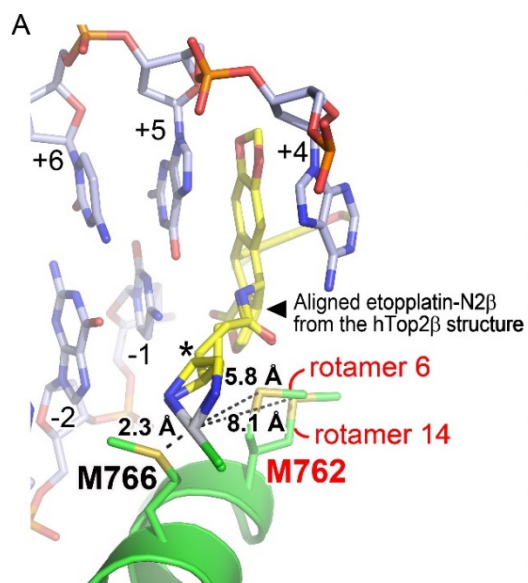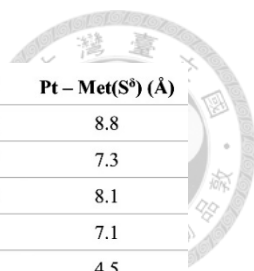
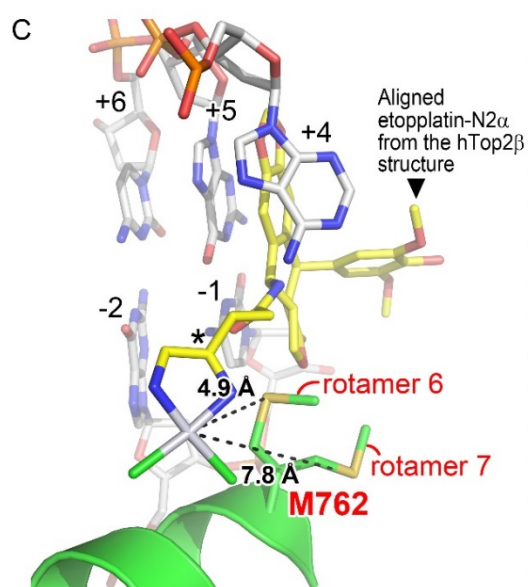| M762 Rotamer #	Chi 1	Chi 2	Chi 3	Pt – Met(S$^\delta$) (Å)
1	-36.8	-50.8	161.8	8.8
2	-68.7	-68.7	-68.7	7.3
3	-61.2	176.3	176.3	8.1
4	-72.5	-72.5	74.7	7.1
5	180.0	-70.0	60.7	4.5
6	176.3	176.3	-62.0	5.8
7	-72.5	74.7	106.9	9.4
8	-70.0	60.7	180.0	9.4
9	-68.7	-68.7	-171.9	7.3
10	176.3	-62.0	172.5	4.5
11	74.7	106.9	-72.5	5.8
12	60.7	180.0	-70.0	7.5
13	-68.7	-171.9	-171.9	7.7
14	-62.0	172.5	172.5	8.1

B
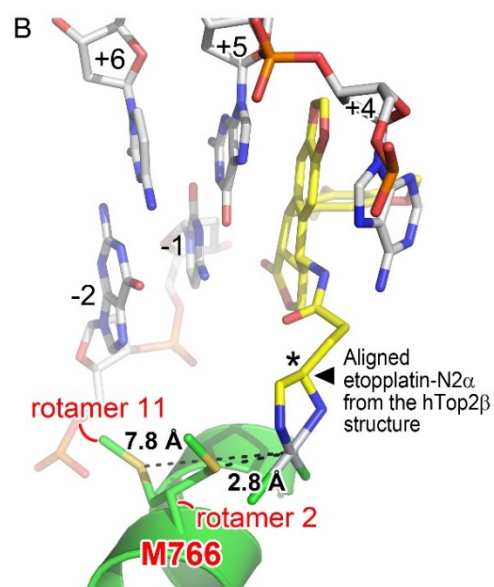
M766 Rotamer #	Chi 1	Chi 2	Chi 3	Pt – Met(S$^\delta$) (Å)
1	-90.2	-104.3	-37.0	4.0
2	-68.7	-68.7	-68.7	2.8
3	-61.2	176.3	176.3	4.4
4	-72.5	-72.5	74.7	3.0
5	180.0	-70.0	60.7	7.2
6	176.3	176.3	-62.0	6.2
7	-72.5	74.7	106.9	3.9
8	-70.0	60.7	180.0	3.8
9	-68.7	-68.7	-171.9	2.8
10	176.3	-62.0	172.5	7.2
11	74.7	106.9	-72.5	7.8
12	60.7	180.0	-70.0	7.2
13	-68.7	-171.9	-171.9	4.2
14	-62.0	172.5	172.5	4.4

C

M762 Rotamer #	Chi 1	Chi 2	Chi 3	Pt – Met(S$^\delta$) (Å)
1	-61.9	-172.5	172.49	6.8
2	-68.7	-68.7	-68.7	5.3
3	-61.2	176.3	176.3	6.7
4	-72.5	-72.5	74.7	5.0
5	180.0	-70.0	60.7	4.3
6	176.3	176.3	-62.0	4.9
7	-72.5	74.7	106.9	7.8
8	-70.0	60.7	180.0	7.8
9	-68.7	-68.7	-171.9	5.3
10	176.3	-62.0	172.5	4.3
11	74.7	106.9	-72.5	5.7
12	60.7	180.0	-70.0	7.0
13	-68.7	-171.9	-171.9	6.3
14	-62.0	172.5	172.5	6.8

73

Figure 17. Structural models of the hTop2α cleavage complexes stabilized by etoplatins.

(A) The modeled structure of hTop2α^{core}- DNA-etoplatin-N2β revealed that the side-chain S^δ of M766 (equivalent to M782 of hTop2β) may contact the coordination sphere of Pt^{2+} to allow the formation of a Pt^{2+}-S coordinate bond (left), consistent with the finding that etoplatin-N2β acts as an irreversible poison of hTop2α. In contrast, Pt^{2+} is not likely to form a coordinate bond with M762 because, for all possible rotamers, the positions of its side-chain S^δ are too distant to react with Pt^{2+} (right). (B, C) The modeled structure of hTop2α^{core}-DNA-etoplatin-N2α suggests that neither M766 nor M762 would form coordinate bond with the Pt^{2+} of etoplatin-N2α. For all possible rotamers, the estimated distances between Pt^{2+} and the S^δ of M766 (B, right) and M762 (C, right) are too long to allow coordinate bond formation. For simplicity, only selected rotamers whose S^δ points directly at Pt^{2+} without the presence of intervening ε methyl group are shown.
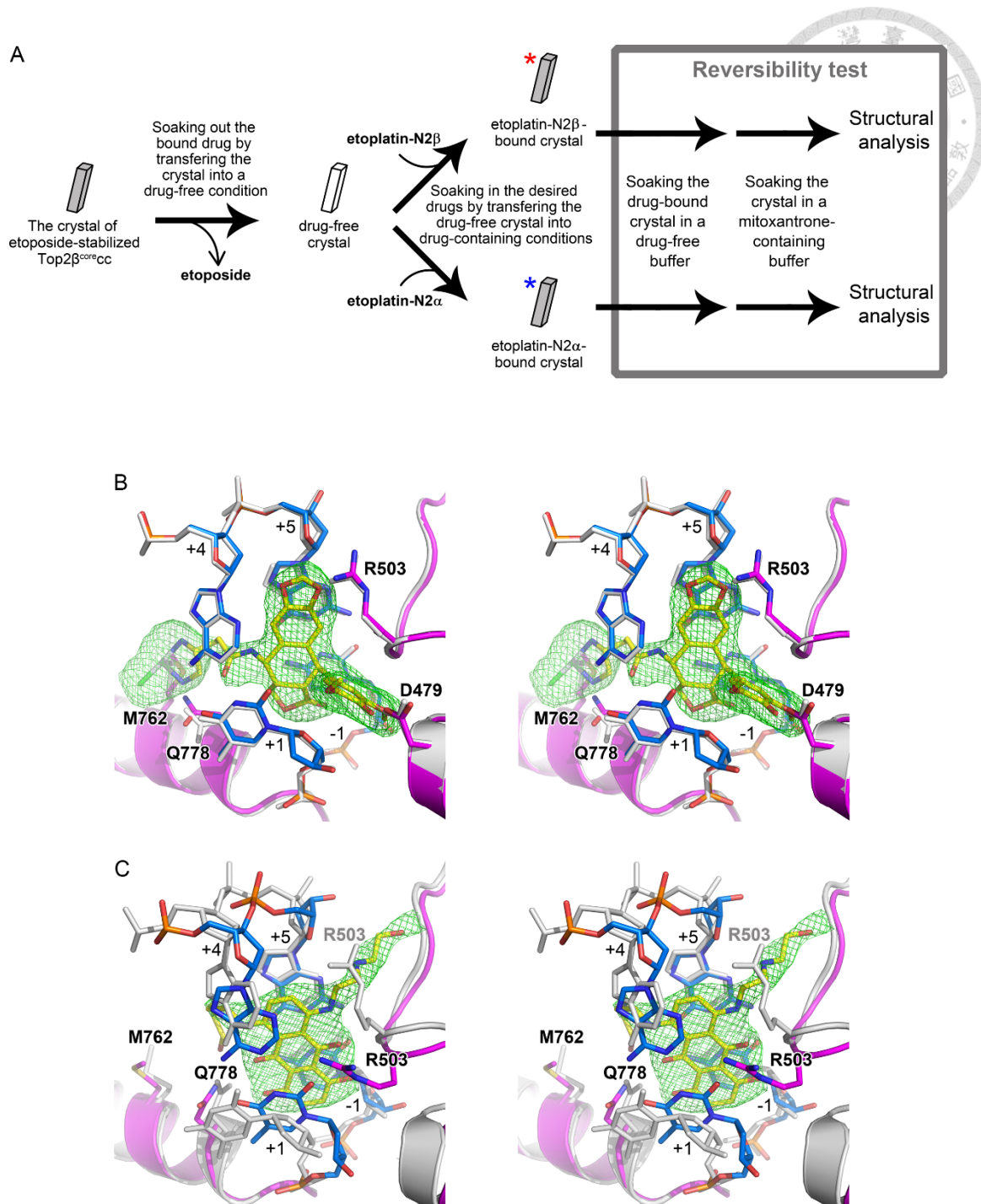
74

Figure 18. Examining the susceptibility of the bound etoplatin-N2α and -N2β to drug replacement.

(A) The experimental scheme for drug replacement and reversibility test. (B and C) The resultant omit (mF_o-DF_c) electron density maps of the bound drug (at 3.0 σ, in green meshes) after subjecting the etoplatin-N2β (or N2α) bound hTop2β^{core}-DNA crystals

75

(marked with red and blue asterisks, respectively, in panel A) to the reversibility test. The

resulting electron density maps show clearly that etoplatin-N2β is resistant to drug

replacement and remained tightly bound (B), while etoplatin-N2α dissociated from the

drug binding site and was replaced by mitoxantrone (C). The parental etoplatin-N2α and

-N2β-bound structures and the post-soaking structures are shown in gray and purple,

respectively. DNA of the resultant structures are shown in blue sticks representation. The

bound etoplatin-N2β (resolution 2.5 Å, panel B) and mitoxantrone (resolution 2.4 Å,

panel C) were modeled according to the features shown in the omit maps and are

displayed in yellow sticks representation. The observed repositioning of the R503 side

chain upon the binding of mitoxantrone was also detected in the mitoxantrone-bound
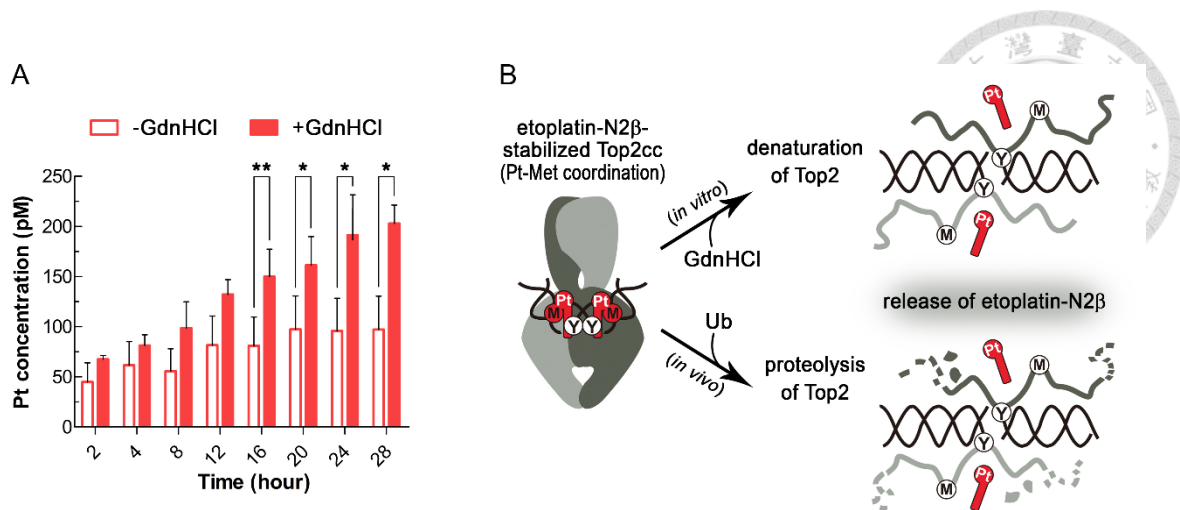
hTop2βcc structure determined previously (54).

76

Figure 19. The etoplatin-N2β-mediated Pt^{2+}-thioether coordination relies on the integrity of hTop2cc structure.

(A) The release of etoplatin-N2β (as reflected by the amount of membrane permeable Pt^{2+}) from structurally intact (-GdnHCl) and denatured (+GdnHCl) Top2cc derived from hTop2α$^{FL-ΔCTD}$ was quantified by ICP-MS. The membrane permeable Pt^{2+} level of the +GdnHCl group gradually increases with time and was significantly higher than the -GdnHCl group started from 16 hour. (*: P<0.05, **: P<0.01) (B) Cartoon representations illustrating that the release of etoplatin-N2β from Top2cc upon GdnHCl treatment (*in vitro* route) may be achieved by targeting Top2 to the 26S proteasome for degradation (*in vivo* route). Specifically, the trapped Top2cc on genomic DNA in the cell will be ubiquitinated (Ub) and channeled to the 26S proteasome for degradation (40,81). Upon structural disruption of its binding site, etoplatin-N2β can no longer form stable coordination with the targeting methionine, allowing its release from the protein.
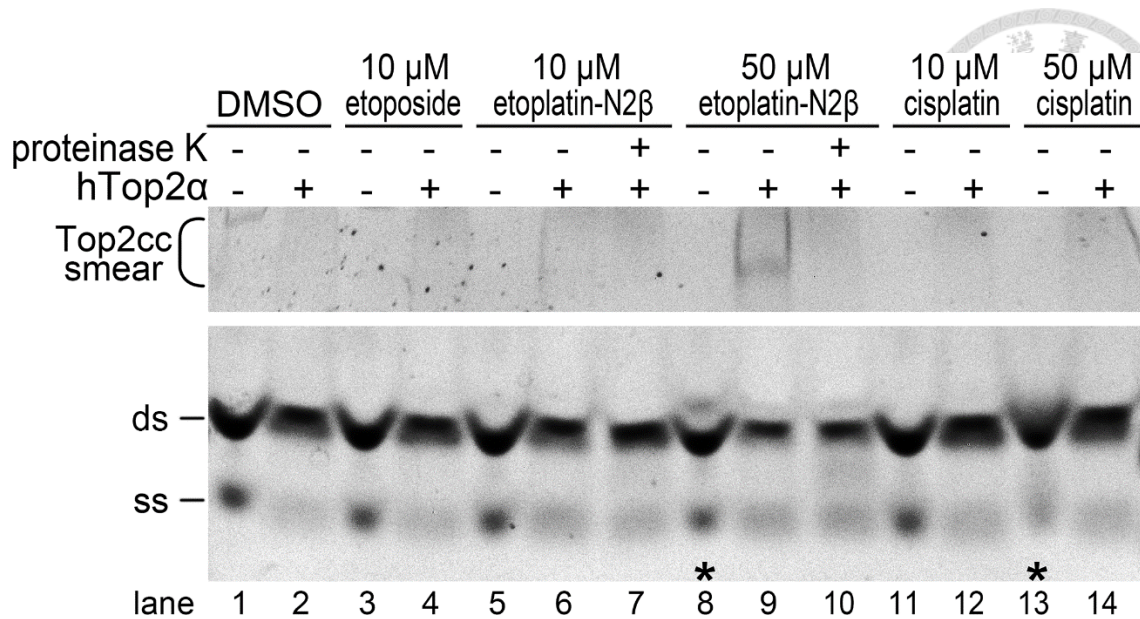
Figure 20. Electrophoretic mobility shift assay (EMSA).

The etoplatin-N2β preferentially binds to and stabilizes Top2cc rather than forming drug-DNA adduct like cisplatin. 600 nM of a 30-bp duplex DNA with residual single strand DNA was used for each lane. For the enzyme-positive lanes, 600 nM of hTop2α was added. Only selected regions showing the presence of slow-migrating Top2cc (upper panel) and the fast migrating DNA substrates (lower panel) are displayed in this figure. Lanes showing the presence of drug-stabilized Top2cc and drug-DNA adduct are specified by *.

Figure 21. Superimposition of drug binding pocket of hTop2α^{core}-DNA-MIX and hTop2β^{core}-DNA-MIX.
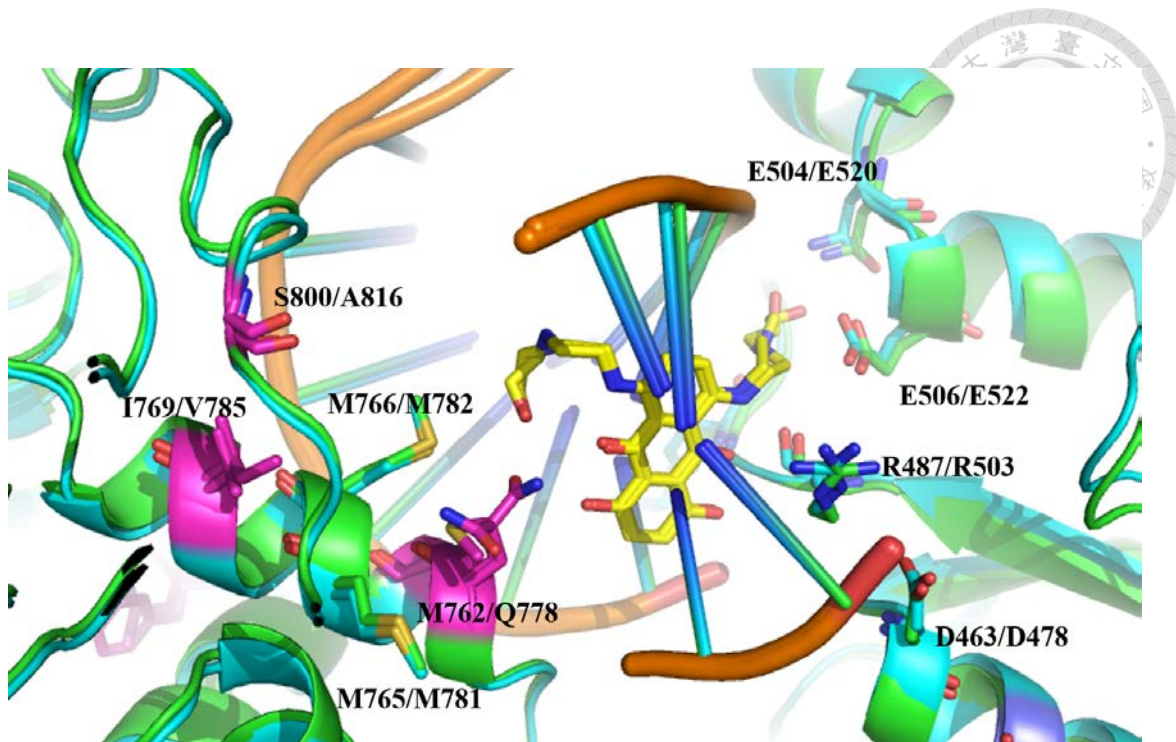
In the well alignment active site, there are only 3 different residues S800/A816、I769/V785 and M762/Q778 in hTop2α/hTop2β in the drug binding site. The hTop2α^{core}-DNA-MIX color show in green, and hTop2β^{core}-DNA-MIX color show in cyan.
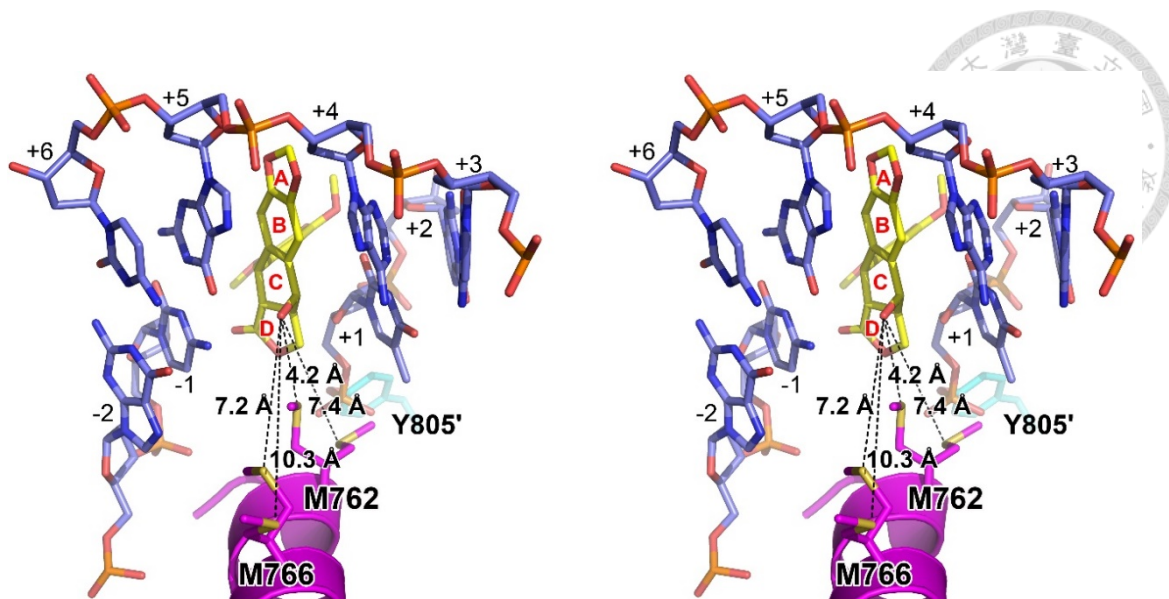
79

Figure 22. Stereo view of the major groove-binding pocket in the etoposide-stabilized hTop2αcc structure.

DNA is shown as blue sticks. Protein is shown in cartoon/stick presentation with the two polypeptide chains colored differently (magenta and cyan). For clearance, the sugar moiety of the bound etoposide (yellow sticks) is omitted from the model. Depending on rotamer conformations adopted by the methionine side chains, the estimated distances between the C-ring-attached hydroxyl group of the bound etoposide and the sulfur atoms of the flanking methionines (M762: 4.2~7.4 Å; M766: 7.2~10.3 Å) are labeled and illustrated by the black dashed lines. Given that M762 and M766 occupy distinct spatial locations, it should be achievable to design a site-specific methionine-targeting by adjusting the length of the Pt^{2+}-coordinating diammine linker such that Pt^{2+} specifically coordinates with M762, which would allow hTop2α-selective targeting.

80
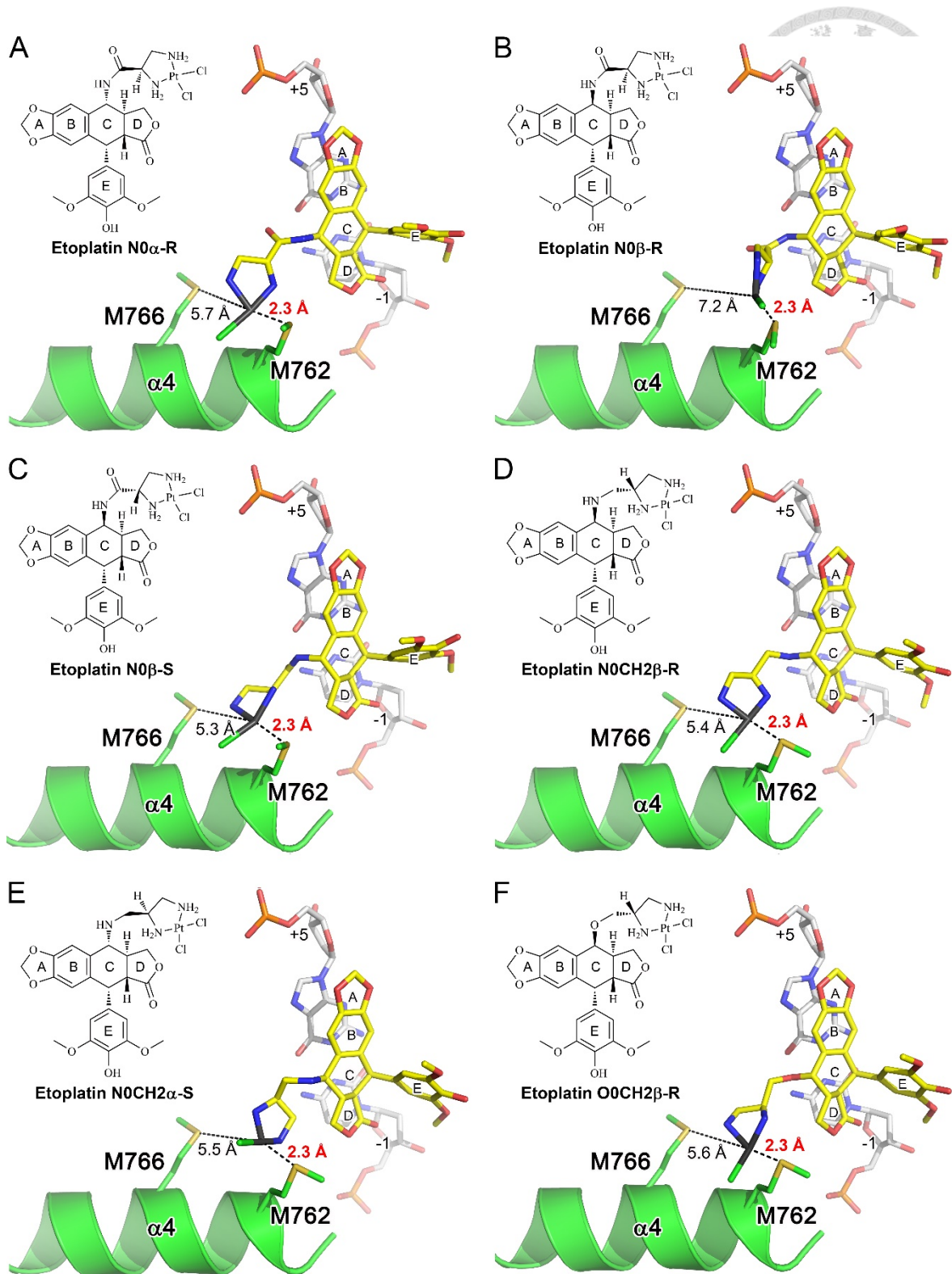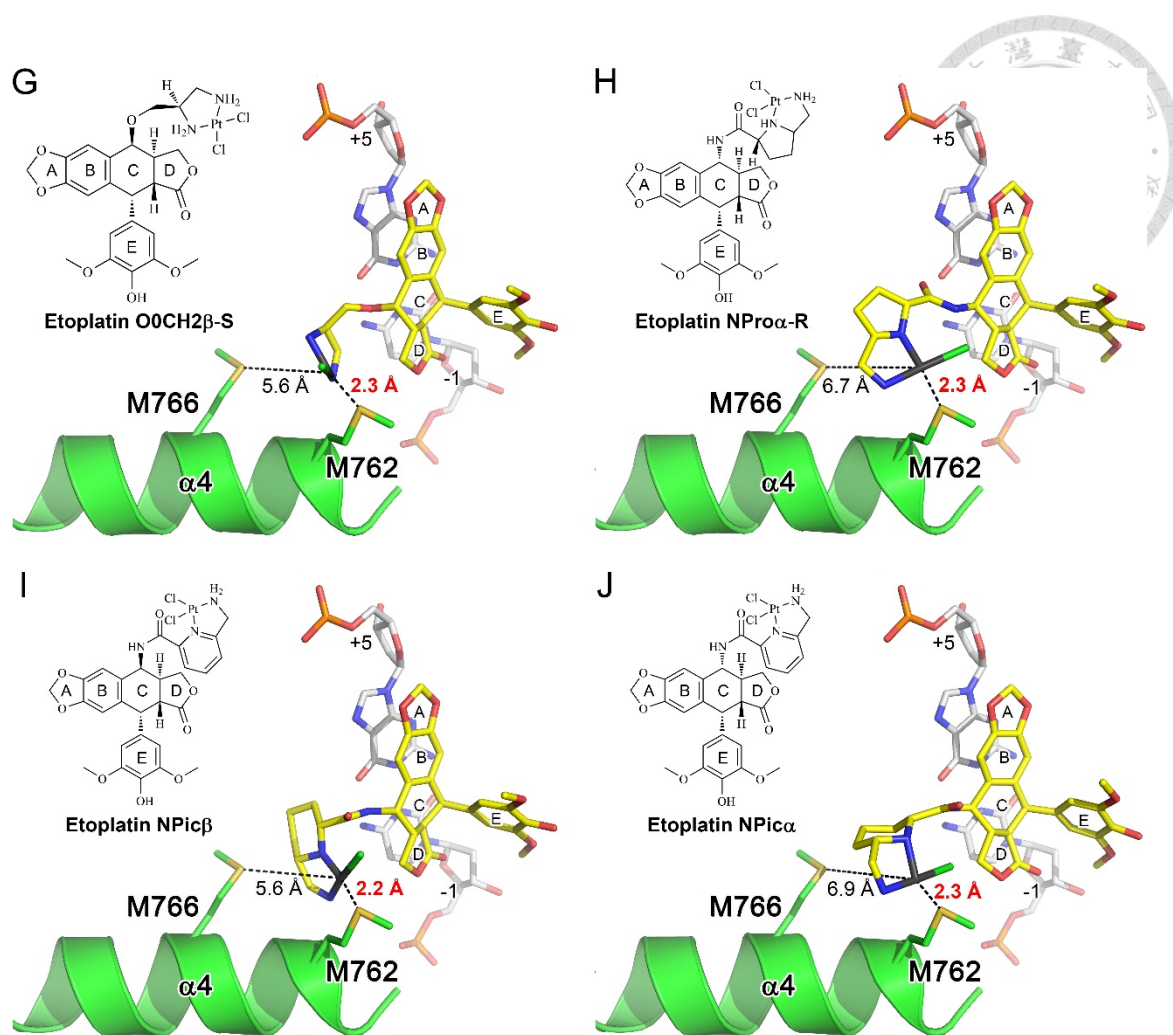
Figure 23. Simulated targeting of the hTop2α-specific M762 by newly designed etoplatins.

(A~J) Each panel shows the structure and a simulated binding mode of a synthesizable, new generation of etoplatin. The etoplatins are colored by atom type (carbon, yellow; oxygen, red; nitrogen, blue; sulfur, yellow; chloride, green; Pt^{2+}, dark grey).This modeling analysis showed that, by adjusting the linker structure and length, Pt^{2+} can be delivered to ~2.3 Å from the S^δ of M762 to allow coordinate bond formation. In contrast, the S^δ of M766 was found to lie at least 5 Å away from Pt^{2+} and thus unable to serve as a ligand.
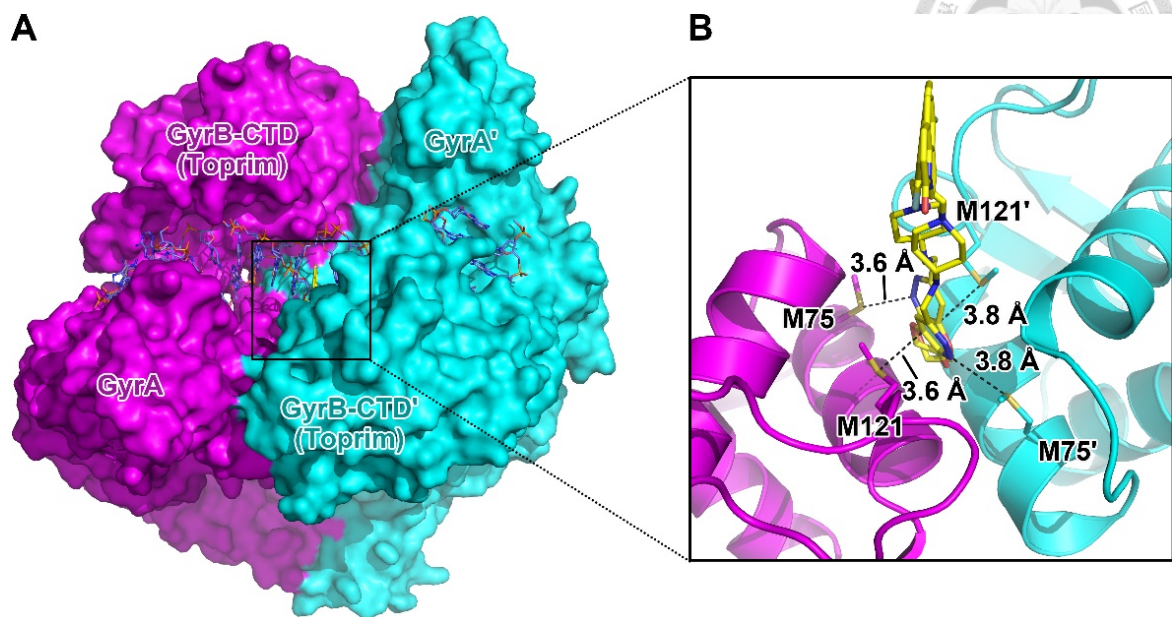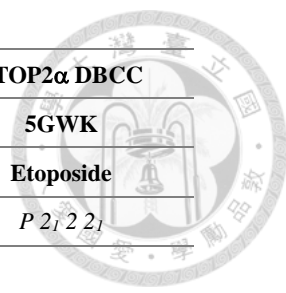
Figure 24. The GSK945237-stabilized gyrase-DNA complex (PDBid: 5IWI).

(**A**) The top view of the overall structure. Gyrase, a bacterial Top2, is assembled as a symmetric $(GyrA)_2(GyrB)_2$ heterotetramer. For clarity, the two symmetric halves are colored in purple and cyan. Labels belong to the second symmetric unit are flagged by a prime. DNA is shown in blue sticks. The bound GSK945237 (in dual conformation) is shown in yellow sticks. (**B**) The enlarged view reveals the presence of four methionine residues surrounding the bound GSK945237 (in sticks). Distances between the sulfur atoms of methionine side chains and the bound drug are indicated.

6. Tables and Scheme

Protein	hTOP2β DBCC		hTOP2α DBCC
PDB ID code	**5GWJ**	**5GWI**	**5GWK**
Ligand	**Etoplatin N2β**	**Etoplatin N2α**	**Etoposide**
Space group	*P 1 2₁ 1*		*P 2₁ 2 2₁*
Unit cell dimensions			
a, b, c **(Å),**	80.18, 177.0, 94.41,	79.79, 176.97, 94.53,	105.11, 126.16. 198.86
β (degrees)	111.5	112.3	
Data collection			
Resolution range (Å)	29.64-2.57 (2.66-2.57)	29.68-2.74 (2.84-2.74)	27.42-3.15 (3.27-3.15)
Observed reflections	290555 (1051)	226170 (885)	309096 (412)
Unique reflections	77673 (7441)	62535 (6108)	45909 (4494)
Multiplicity	3.7 (3.7)	3.6 (3.4)	6.7 (6.7)
Completeness (%)	99.9 (99.8)	98.2 (96.7)	99.2 (99.7)
Mean I/sigma(I)	15.7 (2.8)	13.6 (3.0)	24.6 (3.7)
Rsym[a] (last shell) (%)	0.08 (0.484)	0.087 (0.469)	0.062 (0.48)
Data refinement			
WilsonB-factor	39.94	49.32	92.61
R-crys[b] (%)	0.18	0.21	0.20
R-free[b] (%)	0.22	0.25	0.24
RMSD (bonds)	0.004	0.002	0.002
RMSD (angles)	0.743	0.526	0.566
Ramachandran[c]			
favored (%)	96.5	96.5	96.1
outliers (%)	0.0	0.0	0.0
Clashscore	3.54	3.16	3.26
Average B-factor	46.6	51.7	108.1

Table 1. Summary of hTop2β[core]-DNA-etoplatin ternary complex crystallographic

analysis.

Statistics for the highest-resolution shell are shown in parentheses.
[a]Rsym = ($\sum$ |Ihkl - $\langle$ I $\rangle$ |)/($\sum$ Ihkl), where the average intensity $\langle$ I $\rangle$ is taken overall symmetry equivalent measurements, and Ihkl is the measured intensity for any given reflection.
[b]Rcryst = (Σ||Fo| - k|Fc||)/(Σ|Fo|). Rfree = Rcryst for a randomly selected subset (5%) of the data that were not used for minimization of the crystallographic residual.
[c]Categories were defined by PHENIX. All non-glycine residues are included for this analysis.

Protein	hTOP2β DBCC		hTOP2α DBCC
Ligand	Etoplatin N2β	Etoplatin N2α	Etoposide
Space group	*P 1 2₁ 1*		*P 2₁ 2 2₁*
Unit cell dimensions			
a, *b*, *c* (Å),	80.18, 177.0, 94.41,	79.79, 176.97, 94.53,	105.11, 126.16. 198.86
β (degrees)	111.5	112.3	
Data collection			
Resolution range (Å)	29.64-2.57 (2.66-2.57)	29.68-2.74 (2.84-2.74)	27.42-3.15 (3.27-3.15)
Observed reflections	290555 (1051)	226170 (885)	309096 (412)
Unique reflections	77673 (7441)	62535 (6108)	45909 (4494)
Multiplicity	3.7 (3.7)	3.6 (3.4)	6.7 (6.7)
Completeness (%)	99.9 (99.8)	98.2 (96.7)	99.2 (99.7)
Mean I/sigma(I)	15.7 (2.8)	13.6 (3.0)	24.6 (3.7)
Rsym[a] (last shell) (%)	0.08 (0.484)	0.087 (0.469)	0.062 (0.48)
Data refinement			
WilsonB-factor	39.94	49.32	92.61
R-crys[b] (%)	0.18	0.21	0.20
R-free[b] (%)	0.22	0.25	0.24
RMSD (bonds)	0.004	0.002	0.002
RMSD (angles)	0.743	0.526	0.566
Ramachandran[c]			
favored (%)	96.5	96.5	96.1
outliers (%)	0.0	0.0	0.0
Clashscore	3.54	3.16	3.26
Average B-factor	46.6	51.7	108.1

Table 2. Summary of hTop2α^{core}-DNA-drug ternary complex crystallographic analysis.
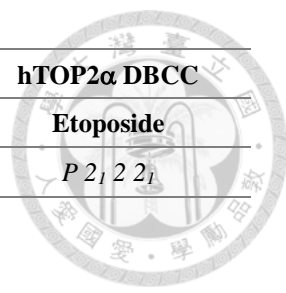
Statistics for the highest-resolution shell are shown in parentheses.
[a]Rsym = ($\sum$|Ihkl - $\langle$I$\rangle$|)/($\sum$Ihkl), where the average intensity $\langle$I$\rangle$ is taken overall symmetry equivalent measurements, and Ihkl is the measured intensity for any given reflection.
[b]Rcryst = (Σ||Fo| - k|Fc||)/(Σ|Fo|). Rfree = Rcryst for a randomly selected subset (5%) of the data that were not used for minimization of the crystallographic residual.
[c]Categories were defined by PHENIX. All non-glycine residues are included for this analysis.

Scheme S1. Synthesis of platinum(II)-4,5-diaminovaleric acid complex (PtCl₂(*N,N*-Dav)) (2)
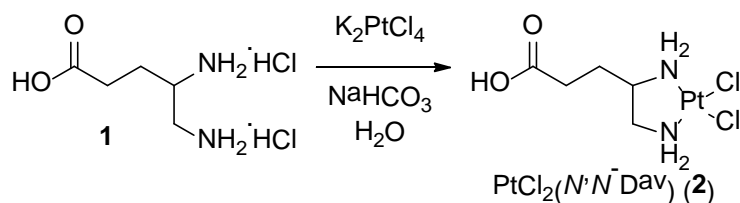
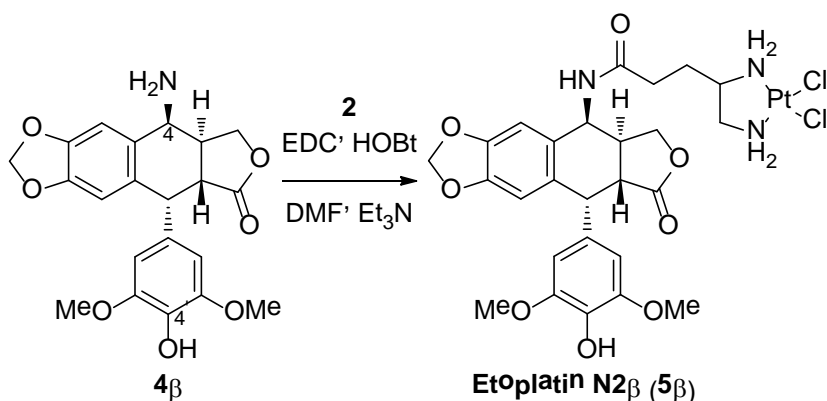$$\text{PtCl}_2(N,N\text{-Dav}) \ (\mathbf{2})$$

Platinum(II)-4,5-diaminovaleric acid complex (PtCl₂(*N,N*-Dav)) (2) (67)

To a mixture of 4,5-diaminovaleric acid dihydrochloride (**1**, 250 mg, 1.22 mmol) in H_2O (10 mL) was added $NaHCO_3$ (205 mg, 2.44 mmol). The mixture was stirred at room temperature for 10 min then K_2PtCl_4 (0.506 g, 1.22 mmol, 1 equiv) was added. The reaction mixture was heated at 80 ^{o}C under N_2 overnight. The reaction mixture was cooled to room temperature and a yellow solid formed. The precipitate was filtered and dried to give a yellow solid (320 mg). The crude product was used for the subsequent reaction without further purification.
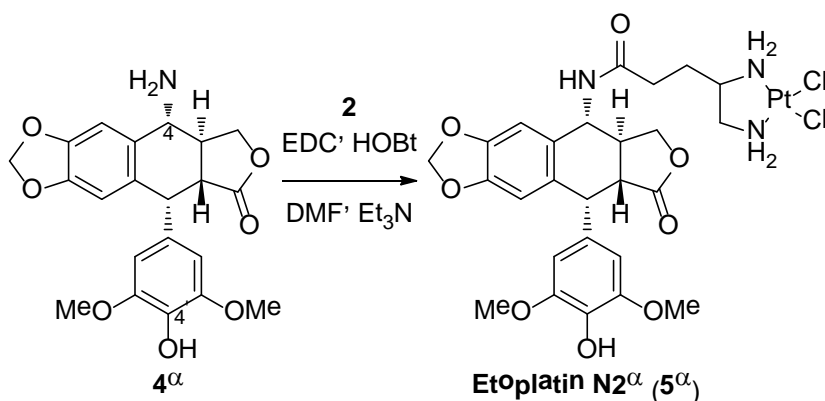
87

Scheme S2. Synthesis of etoplatin-N2β (5β)

Etoplatin-N2β (5β)

To a mixture of PtCl$_2$(*N*,*N*-Dav)(67) (**2**, 239 mg, 0.6 mmol), (*4S*)-4-amino-4-deoxy-4'-*O*-demethylpodophyllotoxin(68) (**4β**, 200 mg, 0.5 mmol), EDCI (144 mg, 0.75 mmol) and HOBT (108 mg, 0.8 mmol) in DMF (15 mL) was added Et$_3$N (101 mg, 1.0 mmol) at room temperature. The mixture was stirred at room temperature overnight. The reaction mixture was extracted with ethyl acetate and the organic layer was concentrated. The crude product was purified by preparative HPLC (ACN/H$_2$O, 15-40%, 25 min) to give etoplatin-N2β (**5β**, yellow solid, 160 mg, 41%). ^{1}HNMR (DMSO-*d$_6$*, 400 MHz) δ 8.25 (s, 1 H), 8.22 (d, 1 H, *J* = 8.2 Hz), 6.77 (s, 1 H), 6.53 (s, 1 H), 6.24 (s, 2 H), 6.02 (s, 1 H), 5.99 (s, 1 H), 5.54-5.53 (m, 1 H), 5.36-5.29 (m, 2 H), 5.15 (dd, 1 H, *J* = 4.6, 8.1 Hz), 5.08 (t, 1 H, *J* = 9.7 Hz), 4.49 (d, 1 H, *J* = 5.1 Hz), 4.27 (t, 1 H, *J* = 8.0 Hz), 3.70 (dd, 1 H, *J* = 8.9, 10.6 Hz), 3.63 (s, 6 H), 3.12 (dd, 1 H, *J* = 5.2, 14.4 Hz), 2.97-2.89 (m, 1 H), 2.60-2.57 (m, 1 H), 2.37-2.35 (m, 1 H), 2.20-2.12 (m, 3 H), 1.81-1.74 (m, 2 H); ^{13}CNMR (DMSO-*d$_6$*, 100 MHz) δ 174.87, 171.89, 147.61, 146.98, 135.23, 132.62, 130.83, 130.56, 109.84, 109.40, 109.00, 101.65, 68.77, 59.67, 56.47, 50.88, 47.09, 43.30, 41.37, 36.95, 32.48, 26.95; MS (ESI) m/z 780 (100) (M+2); HRMS (ESI, TOF) calcd for C$_{26}$H$_{31}$Cl$_2$N$_3$O$_8$Pt (M$^+$): 778.1136. Found: 778.1124.

Scheme S3. Synthesis of etoplatin-N2α (5α)

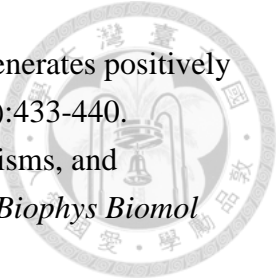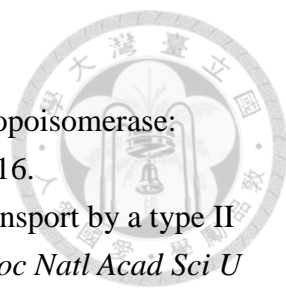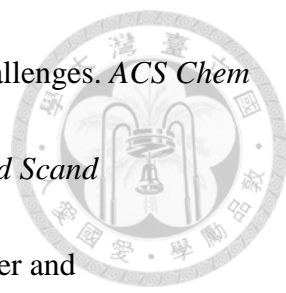**Etoplatin-N2α (5α)**

To a mixture of PtCl$_2$(*N,N*-Dav)(67) (**2**, 239 mg, 0.6 mmol), (*4R*)-4-amino-4-deoxy-4'-*O*-demethylpodophyllotoxin(68) (**4α**, 200 mg, 0.5 mmol), EDCI (144 mg, 0.75 mmol) and HOBT (108 mg, 0.8 mmol) in DMF (15 mL) was added Et$_3$N (101 mg, 1.0 mmol) at room temperature. The mixture was stirred at room temperature overnight. The reaction mixture was extracted with ethyl acetate and the organic layer was concentrated. The crude product was purified by preparative HPLC (ACN/H$_2$O, 15-40%, 25 min) to give etoplatin-N2α (**5α**, pale yellow solid, 150 mg, 38%). ^{1}HNMR (DMSO-*d$_6$*, 400 MHz) δ 8.45 (d, 1 H, *J* = 8.0 Hz), 8.25 (s, 1 H), 6.81 (s, 1 H), 6.52 (s, 1 H), 6.36 (s, 2 H), 5.99 (s, 2 H), 5.53-5.51 (m, 1 H), 5.35-5.31 (m, 2 H), 5.11 (t, 1 H, *J* = 9.4 Hz), 4.95 (t, 1 H, *J* = 9.1 Hz), 4.47 (d, 1 H, *J* = 4.6 Hz), 4.30 (t, 1 H, *J* = 7.6 Hz), 4.06 (t, 1 H, *J* = 9.6 Hz), 3.68 (s, 6 H), 3.23 (dd, 1 H, *J* = 4.9, 14.2 Hz), 2.69-2.61 (m, 2 H), 2.37-2.31 (m, 1 H), 2.29-2.24 (m, 2 H), 2.16-2.15 (m, 1 H), 1.89-1.75 (m, 2 H); ^{13}CNMR (DMSO-*d$_6$*, 100 MHz) δ 175.00, 172.69, 147.60, 146.96, 135.29, 132.46, 131.58, 131.33, 110.19, 109.47, 106.71, 101.57, 71.09, 59.59, 56.78, 51.66, 51.18, 45.26, 43.50, 38.85, 32.60, 27.00; MS (ESI) m/z 780 (100) (M+2); HRMS (ESI, TOF) calcd for C$_{26}$H$_{31}$Cl$_2$N$_3$O$_8$Pt (M$^+$): 778.1136. Found: 778.1133.
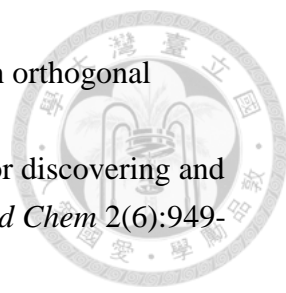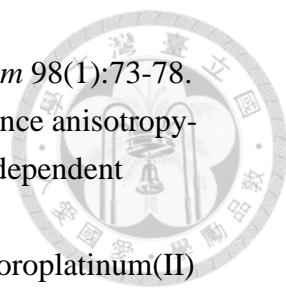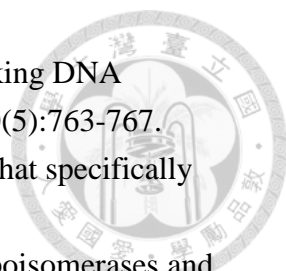
7. Reference

1. Wu HY, Shyy SH, Wang JC, & Liu LF (1988) Transcription generates positively and negatively supercoiled domains in the template. *Cell* 53(3):433-440.

2. Corbett KD & Berger JM (2004) Structure, molecular mechanisms, and evolutionary relationships in DNA topoisomerases. *Annu Rev Biophys Biomol Struct* 33:95-118.

3. Champoux JJ (2001) DNA topoisomerases: structure, function, and mechanism. *Annu Rev Biochem* 70:369-413.

4. Rodriguez AC (2002) Studies of a positive supercoiling machine. Nucleotide hydrolysis and a multifunctional "latch" in the mechanism of reverse gyrase. *J Biol Chem* 277(33):29865-29873.

5. Wang JC (1996) DNA topoisomerases. *Annu Rev Biochem* 65:635-692.

6. Vos SM, Tretter EM, Schmidt BH, & Berger JM (2011) All tangled up: how cells direct, manage and exploit topoisomerase function. *Nat Rev Mol Cell Biol* 12(12):827-841.

7. Gadelle D, Filee J, Buhler C, & Forterre P (2003) Phylogenomics of type II DNA topoisomerases. *Bioessays* 25(3):232-242.

8. Forterre P, Gribaldo S, Gadelle D, & Serre MC (2007) Origin and evolution of DNA topoisomerases. *Biochimie* 89(4):427-446.

9. Bergerat A, Gadelle D, & Forterre P (1994) Purification of a DNA topoisomerase II from the hyperthermophilic archaeon Sulfolobus shibatae. A thermostable enzyme with both bacterial and eucaryal features. *J Biol Chem* 269(44):27663-27669.

10. Bergerat A*, et al.* (1997) An atypical topoisomerase II from Archaea with implications for meiotic recombination. *Nature* 386(6623):414-417.

11. Schoeffler AJ & Berger JM (2005) Recent advances in understanding structure-function relationships in the type II topoisomerase mechanism. *Biochem Soc Trans* 33(Pt 6):1465-1470.

12. Nitiss JL (2009) DNA topoisomerase II and its growing repertoire of biological functions. *Nat Rev Cancer* 9(5):327-337.

13. Kato J*, et al.* (1990) New topoisomerase essential for chromosome segregation in E. coli. *Cell* 63(2):393-404.

14. Dutta R & Inouye M (2000) GHKL, an emergent ATPase/kinase superfamily. *Trends Biochem Sci* 25(1):24-28.

15. Wigley DB, Davies GJ, Dodson EJ, Maxwell A, & Dodson G (1991) Crystal structure of an N-terminal fragment of the DNA gyrase B protein. *Nature* 351(6328):624-629.

16. Corbett KD & Berger JM (2003) Structure of the topoisomerase VI-B subunit: implications for type II topoisomerase mechanism and evolution. *EMBO J*

22(1):151-163.

17. Roca J & Wang JC (1994) DNA transport by a type II DNA topoisomerase: evidence in favor of a two-gate mechanism. *Cell* 77(4):609-616.

18. Roca J, Berger JM, Harrison SC, & Wang JC (1996) DNA transport by a type II topoisomerase: direct evidence for a two-gate mechanism. *Proc Natl Acad Sci U S A* 93(9):4057-4062.

19. Kampranis SC, Bates AD, & Maxwell A (1999) A model for the mechanism of strand passage by DNA gyrase. *Proc Natl Acad Sci U S A* 96(15):8414-8419.

20. Williams NL & Maxwell A (1999) Locking the DNA gate of DNA gyrase: investigating the effects on DNA cleavage and ATP hydrolysis. *Biochemistry* 38(43):14157-14164.

21. Austin CA & Marsh KL (1998) Eukaryotic DNA topoisomerase II beta. *Bioessays* 20(3):215-226.

22. McClendon AK & Osheroff N (2007) DNA topoisomerase II, genotoxicity, and cancer. *Mutat Res* 623(1-2):83-97.

23. Deweese JE & Osheroff N (2009) The DNA cleavage reaction of topoisomerase II: wolf in sheep's clothing. *Nucleic Acids Res* 37(3):738-748.

24. Liu Z, Deibler RW, Chan HS, & Zechiedrich L (2009) The why and how of DNA unlinking. *Nucleic Acids Res* 37(3):661-671.

25. Woessner RD, Mattern MR, Mirabelli CK, Johnson RK, & Drake FH (1991) Proliferation- and cell cycle-dependent differences in expression of the 170 kilodalton and 180 kilodalton forms of topoisomerase II in NIH-3T3 cells. *Cell Growth Differ* 2(4):209-214.

26. Christensen MO*, et al.* (2002) Dynamics of human DNA topoisomerases IIalpha and IIbeta in living cells. *J Cell Biol* 157(1):31-44.

27. Yang X, Li W, Prescott ED, Burden SJ, & Wang JC (2000) DNA topoisomerase IIbeta and neural development. *Science* 287(5450):131-134.

28. Heng X & Le WD (2010) The function of DNA topoisomerase IIbeta in neuronal development. *Neurosci Bull* 26(5):411-416.

29. Ju BG*, et al.* (2006) A topoisomerase IIbeta-mediated dsDNA break required for regulated transcription. *Science* 312(5781):1798-1802.

30. Cowell IG*, et al.* (2012) Model for MLL translocations in therapy-related leukemia involving topoisomerase IIbeta-mediated DNA strand breaks and gene proximity. *Proc Natl Acad Sci U S A* 109(23):8989-8994.

31. Nitiss JL (2009) Targeting DNA topoisomerase II in cancer chemotherapy. *Nat Rev Cancer* 9(5):338-350.

32. Pommier Y & Marchand C (2012) Interfacial inhibitors: targeting macromolecular complexes. *Nat Rev Drug Discov* 11(1):25-36.

33. Pommier Y (2013) Drugging topoisomerases: lessons and challenges. *ACS Chem Biol* 8(1):82-95.

34. Hillestad LK (1957) Acute promyelocytic leukemia. *Acta Med Scand* 159(3):189-194.

35. Ketron AC & Osheroff N (2014) Phytochemicals as Anticancer and Chemopreventive Topoisomerase II Poisons. *Phytochem Rev* 13(1):19-35.

36. Hasan SK, *et al.* (2008) Molecular analysis of t(15;17) genomic breakpoints in secondary acute promyelocytic leukemia arising after treatment of multiple sclerosis. *Blood* 112(8):3383-3390.

37. Deweese JE, Osheroff MA, & Osheroff N (2008) DNA Topology and Topoisomerases: Teaching a "Knotty" Subject. *Biochem Mol Biol Educ* 37(1):2-10.

38. Yeh ET & Bickford CL (2009) Cardiovascular complications of cancer therapy: incidence, pathogenesis, diagnosis, and management. *J Am Coll Cardiol* 53(24):2231-2247.

39. Force T & Kolaja KL (2011) Cardiotoxicity of kinase inhibitors: the prediction and translation of preclinical models to clinical outcomes. *Nat Rev Drug Discov* 10(2):111-126.

40. Azarova AM, *et al.* (2007) Roles of DNA topoisomerase II isozymes in chemotherapy and secondary malignancies. *Proc Natl Acad Sci U S A* 104(26):11014-11019.

41. Zhang S, *et al.* (2012) Identification of the molecular basis of doxorubicin-induced cardiotoxicity. *Nat Med* 18(11):1639-1642.

42. Cowell IG & Austin CA (2012) Mechanism of generation of therapy related leukemia in response to anti-topoisomerase II agents. *Int J Environ Res Public Health* 9(6):2075-2091.

43. Felix CA, Kolaris CP, & Osheroff N (2006) Topoisomerase II and the etiology of chromosomal translocations. *DNA Repair (Amst)* 5(9-10):1093-1108.

44. Joannides M & Grimwade D (2010) Molecular biology of therapy-related leukaemias. *Clin Transl Oncol* 12(1):8-14.

45. Joannides M, *et al.* (2011) Molecular pathogenesis of secondary acute promyelocytic leukemia. *Mediterr J Hematol Infect Dis* 3(1):e2011045.

46. Zarzycka B, *et al.* (2016) Stabilization of protein-protein interaction complexes through small molecules. *Drug Discov Today* 21(1):48-57.

47. Singh J, Petter RC, Baillie TA, & Whitty A (2011) The resurgence of covalent drugs. *Nat Rev Drug Discov* 10(4):307-317.

48. Liu Q, *et al.* (2013) Developing irreversible inhibitors of the protein kinase cysteinome. *Chem Biol* 20(2):146-159.

49. Potashman MH & Duggan ME (2009) Covalent modifiers: an orthogonal approach to drug design. *J Med Chem* 52(5):1231-1246.

50. Johnson DS, Weerapana E, & Cravatt BF (2010) Strategies for discovering and derisking covalent, irreversible enzyme inhibitors. *Future Med Chem* 2(6):949-964.

51. Lavergne SN, Park BK, & Naisbitt DJ (2008) The roles of drug metabolism in the pathogenesis of T-cell-mediated drug hypersensitivity. *Curr Opin Allergy Clin Immunol* 8(4):299-307.

52. Uetrecht J (2009) Immune-mediated adverse drug reactions. *Chem Res Toxicol* 22(1):24-34.

53. Wu CC*, et al.* (2011) Structural basis of type II topoisomerase inhibition by the anticancer drug etoposide. *Science* 333(6041):459-462.

54. Wu CC, Li YC, Wang YR, Li TK, & Chan NL (2013) On the structural basis and design guidelines for type II topoisomerase-targeting anticancer drugs. *Nucleic Acids Res* 41(22):10630-10640.

55. Williams KM, Rowan C, & Mitchell J (2004) Effect of amine ligand bulk on the interaction of methionine with platinum(II) diamine complexes. *Inorg Chem* 43(3):1190-1196.

56. van Maanen JM, Retel J, de Vries J, & Pinedo HM (1988) Mechanism of action of antitumor drug etoposide: a review. *J Natl Cancer Inst* 80(19):1526-1533.

57. Relling MV, Evans R, Dass C, Desiderio DM, & Nemec J (1992) Human cytochrome P450 metabolism of teniposide and etoposide. *J Pharmacol Exp Ther* 261(2):491-496.

58. Relling MV*, et al.* (1994) O-demethylation of epipodophyllotoxins is catalyzed by human cytochrome P450 3A4. *Mol Pharmacol* 45(2):352-358.

59. Zhuo X, Zheng N, Felix CA, & Blair IA (2004) Kinetics and regulation of cytochrome P450-mediated etoposide metabolism. *Drug Metab Dispos* 32(9):993-1000.

60. Otwinowski Z, Minor W, & et al. (1997) Processing of X-ray diffraction data collected in oscillation mode. *Methods Enzymol* 276:307-326.

61. Adams PD*, et al.* (2010) PHENIX: a comprehensive Python-based system for macromolecular structure solution. *Acta Crystallogr D Biol Crystallogr* 66(Pt 2):213-221.

62. Emsley P, Lohkamp B, Scott WG, & Cowtan K (2010) Features and development of Coot. *Acta Crystallogr D Biol Crystallogr* 66(Pt 4):486-501.

63. Schrodinger, LLC (2015) The PyMOL Molecular Graphics System, Version 1.8.

64. Ghezzi A, Aceto M, Cassino C, Gabano E, & Osella D (2004) Uptake of antitumor platinum(II)-complexes by cancer cells, assayed by inductively

coupled plasma mass spectrometry (ICP-MS). *J Inorg Biochem* 98(1):73-78.

65. Shapiro AB & Austin CA (2014) A high-throughput fluorescence anisotropy-based assay for human topoisomerase II beta-catalyzed ATP-dependent supercoiled DNA relaxation. *Anal Biochem* 448:23-29.

66. Liu X*, et al.* (2013) Synthesis and anticancer activity of dichloroplatinum(II) complexes of podophyllotoxin. *Bioorg Med Chem Lett* 23(13):3780-3784.

67. Altman J, Wilchek M, & Warshawsky A (1985) Platinum(II) complexes with 2,4-diaminobutyric acid, ornithine, lysine and 4,5-diaminovaleric acid. *Inorganica Chimica Acta* 107(3):165-168.

68. Hansen HF*, et al.* (1993) New compounds related to podophyllotoxin and congeners: synthesis, structure elucidation and biological testing. *Acta Chemica Scandinavica* 47(12):1190-1200.

69. Liu LF, Rowe TC, Yang L, Tewey KM, & Chen GL (1983) Cleavage of DNA by mammalian DNA topoisomerase II. *J Biol Chem* 258(24):15365-15370.

70. Sander M & Hsieh T (1983) Double strand DNA cleavage by type II DNA topoisomerase from Drosophila melanogaster. *J Biol Chem* 258(13):8421-8428.

71. Zechiedrich EL, Christiansen K, Andersen AH, Westergaard O, & Osheroff N (1989) Double-stranded DNA cleavage/religation reaction of eukaryotic topoisomerase II: evidence for a nicked DNA intermediate. *Biochemistry* 28(15):6229-6236.

72. Vann KR, Sedgeman CA, Gopas J, Golan-Goldhirsh A, & Osheroff N (2015) Effects of Olive Metabolites on DNA Cleavage Mediated by Human Type II Topoisomerases. *Biochemistry* 54(29):4531-4541.

73. Barnham KJ, Guo Z, & Sadler PJ (1996) Stabilization of monofunctional platinum-nucleotide adducts: reactions of N-acetyl-L-methionine complexes with guanosine 5'-monophosphate and guanylyl(3'-5')guanosine. *Journal of the Chemical Society Dalton Transactions*:2867-2876.

74. Todd RC & Lippard SJ (2010) Structure of duplex DNA containing the cisplatin 1,2-{Pt(NH3)2}2+-d(GpG) cross-link at 1.77 A resolution. *J Inorg Biochem* 104(9):902-908.

75. Ezoe S (2012) Secondary leukemia associated with the anti-cancer agent, etoposide, a topoisomerase II inhibitor. *Int J Environ Res Public Health* 9(7):2444-2453.

76. Rashidi A & Fisher SI (2013) Therapy-related acute promyelocytic leukemia: a systematic review. *Med Oncol* 30(3):625.

77. Errington F*, et al.* (1999) Murine transgenic cells lacking DNA topoisomerase IIbeta are resistant to acridines and mitoxantrone: analysis of cytotoxicity and cleavable complex formation. *Mol Pharmacol* 56(6):1309-1316.

78. Lopez-Lazaro M, Willmore E, & Austin CA (2007) Cells lacking DNA topoisomerase II beta are resistant to genistein. *J Nat Prod* 70(5):763-767.

79. Toyoda E*, et al.* (2008) NK314, a topoisomerase II inhibitor that specifically targets the alpha isoform. *J Biol Chem* 283(35):23711-23720.

80. Pommier Y, Leo E, Zhang H, & Marchand C (2010) DNA topoisomerases and their poisoning by anticancer and antibacterial drugs. *Chem Biol* 17(5):421-433.

81. Xiao H*, et al.* (2003) The topoisomerase IIbeta circular clamp arrests transcription and signals a 26S proteasome pathway. *Proc Natl Acad Sci U S A* 100(6):3239-3244.

82. Miles TJ*, et al.* (2016) Novel tricyclics (e.g., GSK945237) as potent inhibitors of bacterial type IIA topoisomerases. *Bioorg Med Chem Lett* 26(10):2464-2469.

83. Kobayashi S*, et al.* (2005) EGFR mutation and resistance of non-small-cell lung cancer to gefitinib. *N Engl J Med* 352(8):786-792.

84. Yun CH*, et al.* (2007) Structures of lung cancer-derived EGFR mutants and inhibitor complexes: mechanism of activation and insights into differential inhibitor sensitivity. *Cancer Cell* 11(3):217-227.